Nonradiative decay of the low-lying nuclear isomer ^{229m}Th(3.5 eV) in a metal

E. V. Tkalya*)
Scientific-Research Institute of Nuclear Physics, M. V. Lomonosov Moscow State University, 119899 Moscow, Russia

(Submitted 27 July 1999)
Pis'ma Zh. Éksp. Teor. Fiz. **70**, No. 6, 367–370 (25 September 1999)

A new nonradiative decay channel for the anomalously low-lying isomeric level $3/2^+(3.5\pm1.0\,\text{eV})$ of the ^{229}Th nucleus in a metal via the conduction electrons is examined. The lifetime of the isomer in a metal is calculated. An explanation is given for the experimental results of S. B. Utter *et al.*, Phys. Rev. Lett. **82**, 505 (1999), where the optical radiation spectrum of the indicated isomer was investigated. © *1999 American Institute of Physics*. [S0021-3640(99)00118-8]

PACS numbers: 23.20.Nx, 23.90.+w

The energy of the first excited level in the ^{229}Th nucleus is 3.5 ± 1.0 eV, which is anomalously low for nuclei.[1,2] The unusual properties of the state ^{229m}Th($3/2^+$, 3.5 ± 1.0 eV) have been discussed repeatedly in the literature. These include decay via an electron bridge,[3] the possibility of laser excitation with the production of a population inversion in a system of ^{229}Th nuclei,[4,5] a change induced in the α decay rate of ^{229}Th by low-intensity laser radiation,[6] and others. It has also been noted that the decay probability of the isomer via an electron bridge and the spectrum of emitted photons are sensitive to the chemical environment. For this reason ^{229}Th can serve as a probe for investigating the properties of substances.[3–5]

In this letter we predict another unique property of the isomer ^{229m}Th, specifically: nonradiative decay of the $3/2^+(3.5\pm1.0\,\text{eV})$ level in a metal via the conduction electrons.

^{229m}Th($3/2^+$, 3.5 ± 1.0 eV) nuclei are produced with approximately 2% probability in the α decay of ^{233}U. Let a thin ^{233}U oxide layer, several tens of angstroms thick, be deposited on a metal substrate. The energy of the ^{229}Th recoil nucleus in the α decay of ^{233}U is ~100 keV. Let us follow the ^{229m}Th(3.5 eV) nuclei whose momentum is directed toward the substrate. According to the data of Ref. 7, their range in metals is several tens of atomic layers. A metal of such thickness is virtually transparent to visible-range optical radiation and is not an obstacle for detecting the photons arising as a result of decay of the low-lying isomer ^{229m}Th.

In an isolated Th atom the isomer $3/2^+(3.5\pm1.0\,\text{eV})$ should decay predominantly via the electron-bridge channel.[3] This is an extremely rare case, indeed the only case known, in which a process of third order in the electromagnetic interaction constant e predominates over internal electron conversion, which is a second-order process, in the

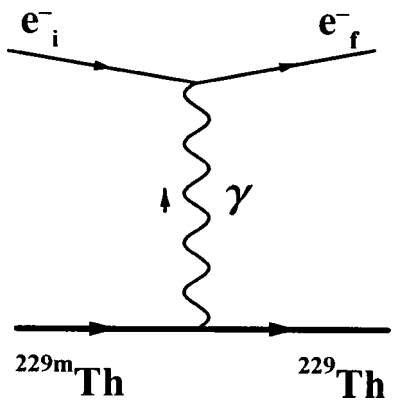

FIG. 1. Diagram of nonradiative decay of ^{229m}Th($3/2^+$, 3.5 ± 1.0 eV) via the conduction electrons in a metal.

decay of a nuclear isomer. Here internal conversion is simply forbidden, since the ionization potential of the Th atom, equal to 6.08 eV, is greater than the energy of the nuclear transition.

The situation changes radically if ^{229m}Th is inserted into a metal. Then the second-order process in which the isomer decays via the conduction electrons, as shown in Fig. 1, becomes allowed. This process is similar to inelastic electron scattering by nuclei. In a metal it does not have an energy threshold, since the nucleus gives up energy in this case. (The threshold of the reaction in semiconductors will be the energy gap. Therefore the energy of the nuclear transition can be determined by varying the substrate material.)

The decay of the isomer in a metal can also be interpreted as conversion on conduction electrons. But here, in contrast to conventional internal conversion, the initial state of the electron is not an atomic bound state.

To estimate qualitatively the decay probability of ^{229m}Th($3/2^+$, 3.5 ± 1.0 eV) in a so-called ''standard'' metal,[8] we shall employ the very simple free-electron approximation[9] (in this model the conduction electrons are treated as a gas of free particles). We shall calculate the probability according to the formula

$$W\sim N_e\, v_e\, \sigma\,,$$

where N_e and v_e are the density and velocity of the conduction electrons and σ is the cross section of the process (the system of units $\hbar=c=1$ is used). Let the energy of the initial state of the electron be $E_i\approx\mathcal{E}_F$, where $\mathcal{E}_F$ is the Fermi energy. Correspondingly, the electron velocity is equal to the Fermi velocity, $v_e\sim v_F=\sqrt{2\mathcal{E}_F/m}$. For inelastic scattering by the isomeric nuclei ^{229m}Th the conduction electrons acquire the additional energy $\omega_N=3.5\pm1.0$ eV. If the electron work function of the metal is less than ω_N, then electrons remain in the metal after being scattered.

To estimate the inelastic scattering cross section σ, we employed a software package[10,11] in which the self-consistent atomic field and the wave functions of bound electrons are found by solving a system of Dirac–Fock equations with allowance for the finite sizes of the nuclei, and the initial and final states of the scattered electron are solutions of the Dirac equation in the indicated field.

The reduced probability of a nuclear isomeric $M1$ transition from the ground into the first excited state of ^{229}Th has been calculated in Ref. 12. With the Coriolis interaction between the rotational bands taken into account (the indicated levels are the bandheads), the value found in Ref. 12 is $B(M1;\ 3/2^+3/2[631]\rightarrow 5/2^+5/2[633])_{W.u.}\simeq 4.8\times 10^{-2}$. On this basis, in order of magnitude we obtain for the cross section $\sigma\sim 10^{-27}\,\mathrm{cm}^2$.

We shall now calculate the decay probability of the isomer ^{229m}Th($3/2^+$, 3.5 ± 1.0 eV) in a standard metal. Using the values $N_e\approx 6\times 10^{22}\,\mathrm{cm}^{-3}$ and $\mathcal{E}_F\approx 5.5$ eV from Ref. 8, we find for the probability $W\sim 10^4\,\mathrm{s}^{-1}$. Therefore the lifetime of a thorium isomer in a metal is $\sim 10^{-4}$ s. The value obtained is much less than the ''reasonable'' lower limit 10^{-2} s found in Ref. 12 for the half-life of the low-lying level of the ^{229}Th nucleus. Therefore the process under consideration can indeed be the dominant decay channel for the state $3/2^+(3.5\pm 1.0\,\mathrm{eV})$ in a metal.

Now the experimental result of Ref. 13 can be interpreted in a completely different way. This experiment differed from the others[14,15] by the fact that the measurements of the optical radiation of ^{229m}Th nuclei were performed in vacuum, and a platinum slab was used as the substrate. The authors of Ref. 13 did not observe the 2.3–2.5 eV photons that had been discovered previously (in 1997–1998) in Refs. 14 and 15, where they had been interpreted as indicating the presence of an electron bridge.

In the vacuum experiment of Ref. 13 the target consisted of a 35 Å thick layer of ^{233}U oxide deposited on a platinum substrate. (We note that metallic substrates were not used in the experiments of Refs. 14 and 15.) The ^{229m}Th recoil nuclei, which entered the chamber at a velocity of 10^{-3}, reached the walls in times not greater than $\sim 10^{-6}$ s and decayed outside the field of view of the optical system. The recoil nuclei ^{229m}Th emerging in the direction of the substrate penetrated into the platinum (their range in Pt is ~ 150 Å)[7] and underwent nonradiative decay via the conduction electrons. The electron work function of platinum is 5.3 eV. Therefore decay likewise could not be recorded by detecting electrons. All this explains the absence of any signal in Ref. 13. Therefore the experimental results of Ref. 13 are consistent with the conjecture made in Refs. 14 and 15 concerning the electron bridge and the ''nuclear'' origin of the 2.3–2.5 eV optical radiation.

If everything occurs as described above, then the experiment of Ref. 13 gives a lower limit for the half-life of ^{229m}Th($3/2^+$, 3.5 ± 1.0 eV): $T_{1/2}\geqslant 1/W\sim 10^{-4}$ s. An upper limit on $T_{1/2}$ can be easily found using the well-known quantity $B(M1)$. When all decay channels, except direct nuclear γ radiation with energy 3.5 eV, are closed, one has $T_{1/2}\simeq 3$ h.

The process studied in this letter, the nonradiative decay of a nuclear isomer in a metal via the conduction electrons, is peculiar to ^{229m}Th($3/2^+$, 3.5 ± 1.0 eV). Nothing like this can be observed for other nuclei. The key element is the smallness of the energy of the isomeric transition and the absence of a conversion decay channel of the isomer in the Th atom. For comparison, consider the ^{235}U nucleus, which possesses the next lowest energy of an isomeric level $1/2^+(76.8\,\mathrm{eV})$, with a lifetime of about 25 min. A calculation of the decay probability of this state in a metal gives $\sim 10^{-6}\,\mathrm{s}^{-1}$. This is approximately three orders of magnitude less than the probability of internal electronic conversion, which is the main decay channel for the isomer $1/2^+(76.8\,\mathrm{eV})$ in ^{235}U.

I thank A. M. Dykhne, N. V. Eremin, A. M. Zherikhin, Yu. E. Lozovik, and V. P. Petukhov for helpful consultations and their interest in this work. This work is supported in part by the Russian Fund for Fundamental Research (Grant No. 98-02-16070a) and a Grant in Support of the Leading Science Schools, No. 96-15-96481.

*)e-mail: tkalya@ibrae.ac.ru

[1] C. W. Reich and R. G. Helmer, Phys. Rev. Lett. **64**, 271 (1990).
[2] R. G. Helmer and C. W. Reich, Phys. Rev. C **49**, 1845 (1994).
[3] V. F. Strizhov and E. V. Tkalya, Zh. Éksp. Teor. Fiz. **99**, 697 (1991) [Sov. Phys. JETP **72**, 387 (1991)].
[4] E. V. Tkalya, Yad. Fiz. **55**, 2881 (1992) [Sov. J. Nucl. Phys. **55**, 1661 (1992)].
[5] E. V. Tkalya, V. O. Varlamov, V. V. Lomonosov, and S. A. Nikulin, Phys. Scr. **53**, 296 (1996).
[6] A. M. Dykhne, N. V. Eremin, and E. V. Tkalya, JETP Lett. **64**, 345 (1996).
[7] A. F. Burenkov, F. F. Komarov, M. A. Kumakhov, and M. M. Temkin, *Spatial Distributions of the Energy Released in an Atomic Collision Cascade in Solids* [in Russian] (Énergoatomizdat, Moscow, 1985).
[8] A. B. Pippard, Rep. Prog. Phys. **23**, 176 (1960).
[9] N. W. Ashcroft and N. D. Mermin, *Solid State Physics* (Holt, Rinehart and Winston, New York, 1976).
[10] I. M. Band, M. A. Listengarten, M. B. Trzhaskovskaya, and V. I. Fomichev, Preprints LIYaF-289 and LIYaF-298–300, Leningrad Institute of Nuclear Physics, Leningrad (1976–1977).
[11] D. P. Grechukhin and A. A. Soldatov, Preprint IAÉ-2976 [in Russian], Kurchatov Institute of Atomic Energy, Moscow (1998).
[12] A. M. Dykhne and E. V. Tkalya, JETP Lett. **67**, 251 (1998).
[13] S. B. Utter, P. Beiersdorfer, A. Barnes *et al.*, Phys. Rev. Lett. **82**, 505 (1999).
[14] G. M. Irwin and K. H. Kim, Phys. Rev. Lett. **79**, 990 (1997).
[15] D. S. Richardson, D. M. Benton, D. E. Evans *et al.*, Phys. Rev. Lett. **80**, 3206 (1998).

Translated by M. E. Alferieff

Coherent Raman scattering in molecular hydrogen in a dc electric field

D. A. Akimov, A. M. Zheltikov, N. I. Koroteev, A. N. Naumov,
A. Yu. Serdyuchenko, D. A. Sidorov-Biryukov, and A. B. Fedotov
P. N. Lebedev Physics Institute, Russian Academy of Sciences, 117924 Moscow, Russia

V. N. Ochkin and S. N. Tskhaĭ
Department of Physics, M. V. Lomonosov Moscow State University, 119899 Moscow, Russia

(Submitted 8 August 1999)
Pis'ma Zh. Éksp. Teor. Fiz. **70**, No. 6, 371–375 (25 September 1999)

The polarization properties of light in coherent Raman scattering in molecular hydrogen in a dc electric field are investigated. A nonlinear polarization-optical method of determining the absolute magnitude and orientation of the dc electric field is proposed and realized. © *1999 American Institute of Physics.* [S0021-3640(99)00218-2]

PACS numbers: 42.65.Dr, 33.80.Wz

Coherent four-photon spectroscopy is an effective method of diagnostics of excited gases and plasma. Specifically, coherent anti-Stokes Raman scattering (CARS)[1,2] is now widely used to measure temperature and concentration in excited gaseous media.[3] As experimental investigations show, coherent four-wave interaction spectroscopy with Raman and hyper-Raman resonances yields important information about the relaxation of the populations of the excited states of atoms and ions and makes it possible to investigate the spatial distributions of resonant particles in laser-produced and gas-discharge plasmas.[4] However, because adequate methods for remote contactless measurement of local electric fields in plasmas are not available, it is difficult to obtain information on a number of important plasma properties. It appears that the rich arsenal of coherent four-photon spectroscopy methods that have been developed to date will make it possible to solve certain problems associated with the measurement of plasma fields. The possibility of using four-photon spectroscopy to measure the intensity of an electric field was proposed in Ref. 5 and experimentally demonstrated in Ref. 6 for a uniform dc electric field with known orientation in a corona-discharge plasma. In Ref. 7 a method for measuring a uniform dc electric field in an isotropic uniform plasma by coherent four-photon scattering was proposed and substantiated theoretically, and the effect of plasma microfields on the intensity and polarization of the four-photon scattering signal was investigated. Coherent four-photon spectroscopy is thus a promising technique for performing local measurements of electric fields in excited gases and plasma.

In the present work the polarization technique of coherent Raman scattering (CRS) is used to perform local contactless measurement of the absolute magnitude and orientation of a dc electric field in molecular gases and to obtain information about the form of

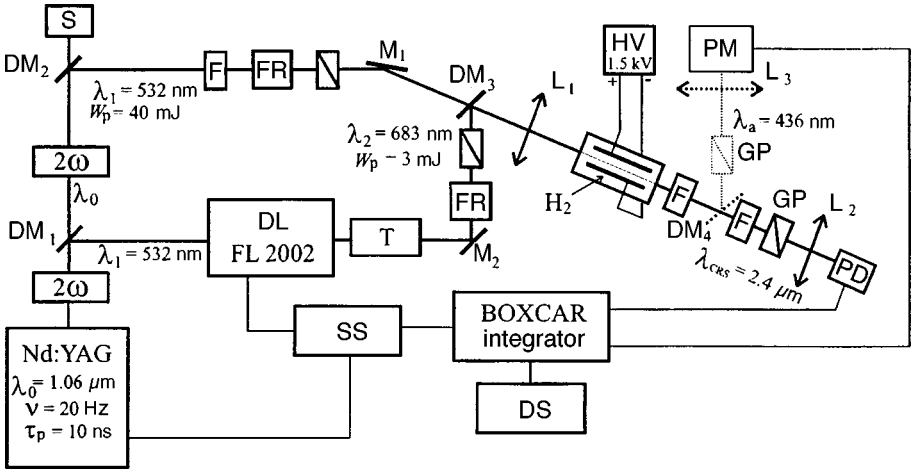

FIG. 1. Experimental setup for investigating CRS in a molecular gas in a dc electric field: Nd:YAG — Nd:YAG laser master oscillator; 2ω — frequency-doubling crystals; DL — dye laser; SS — synchronization system; DS — detection system; PM — photomultiplier; PD — IR detector; T — telescope; M_1, M_2 — rotating mirrors; DM_1–DM_4 — dichroic mirrors; GP — Glan prism; F — light filters; FR — Fresnel rhombs; S — screen; HV — high-voltage source, L_1–L_3 — lenses.

the nonlinear optical susceptibility tensor and the invariants of the Raman scattering tensor of Raman-active transitions of molecules and atoms.

The experimental setup built for investigating CRS processes in a molecular gas in a dc electric field consisted of (see Fig. 1) a master oscillator, crystals for frequency conversion, a dye laser (DL), gas cells, and a detection system. A 1.06 μm Nd:YAG with a 20 Hz pulse repetition frequency and 10 ns pulse duration was used as the master oscillator. A DKDP crystal with 30% efficiency was used to convert radiation into the second harmonic (ω_1 wave). The second-harmonic radiation (532 nm wavelength) was used to pump the dye laser (mixture of pyridine-1 and DCM dyes, dissolved in dimethyl sulfoxide). The dye laser generated radiation with a wavelength of 683 nm (frequency ω_2) and pulse energy 3 mJ. The lasing linewidth of the dye laser was $0.2\,\mathrm{cm}^{-1}$ and the beam diameter was 2.5 mm (0.5 mrad divergence).

The radiation at the fundamental frequency unconverted by the nonlinear crystal was selected by a dichroic mirror DM_1, with approximately 80% transmittance at 532 nm and reflectance exceeding 99% at 1.06 μm, and converted into the second harmonic in a DKDP crystal. The second harmonic obtained in this manner was used as one of the biharmonic pump waves in the CRS scheme (the wave with frequency ω_1). The spectral linewidth of the second-harmonic radiation was $0.2\,\mathrm{cm}^{-1}$, the beam diameter was 7 mm, the beam divergence was 0.6 mrad, and the energy per pulse reached 40 mJ.

After passing through the telescope T, the radiation with frequency ω_2 was combined with the ω_1 beam using a dichroic mirror DM_3. The magnification of the telescope was chosen so as to obtain the optimal ratio between the diameters of the ω_1 and ω_2 beams, and the telescope was set so as to compensate the divergence of the dye-laser radiation.

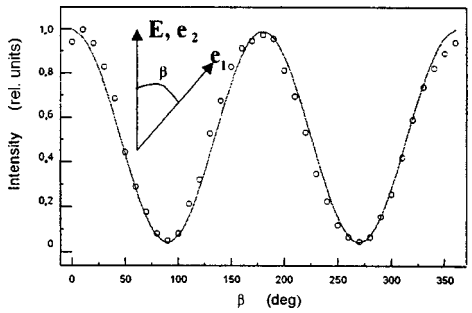

FIG. 2. CRS signal intensity versus the angle β between the polarization vector $\mathbf{e}_1$ of the pump wave and the direction of the dc field $\mathbf{E}$, collinear with the vector $\mathbf{e}_2$. Dots — experimental data. Solid curve — calculation using Eq. (1).

A lens L_1 focused the combined second-harmonic and dye-laser beams into a cell filled with hydrogen under a pressure of about 1.2 atm. Metal electrodes, to which a voltage of 1–1.5 kV was applied, were placed in the cell to produce an electric field.

A system of filters was used to separate from the pump radiation the coherent IR radiation of the CRS signal generated in the region of interaction of the beams and the CARS calibration signal (the calibration procedure is described in Ref. 6). The CRS signal generated as a result of four-photon scattering in the presence of a dc electric field was detected with a liquid-nitrogen-cooled IR detector. The data from the IR detector were accumulated and processed using a BOXCAR integrator and a personal computer. A photomultiplier was used to detect the CARS signal.

In our experiments, a four-photon CRS process, occurring in the presence of a dc electric field E_{dc} according to the scheme $\omega_{\mathrm{CRS}}=\omega_0+\omega_1-\omega_2$, where $\omega_0=0$, ω_1, and ω_2 are the frequencies of the pump waves tuned to a Raman-type resonance with the frequency $\Omega=\omega_1-\omega_2$ of the molecular transition employed ($\lambda_{\mathrm{CRS}}=2.4\,\mu$m, the transition $\nu=0$, $J=1\rightarrow\nu=1$, $J=1$ $H_2(X^1\Sigma_g^+)$), was used to measure the electric field and to investigate the parameters of molecular transitions. In an isotropic medium the polarization vector is determined in terms of the components of the nonlinear optical cubic susceptibility tensor $\chi^{(3)}_{ijkl}=\chi^{(3)}_{ijkl}(\omega_{\mathrm{CRS}};0,\omega_1,-\omega_2)$ and the electric vectors of the pump waves by the following expression[1] (the frequency arguments are dropped in the components of the nonlinear susceptibility tensor):

$$\mathbf{P}^{(3)}=3\{\chi^{(3)}_{1122}\mathbf{E}(\mathbf{e}_1\cdot\mathbf{e}_2^*)+\chi^{(3)}_{1212}\mathbf{e}_1(\mathbf{E}\cdot\mathbf{e}_2^*)+\chi^{(3)}_{1122}\mathbf{e}_2^*(\mathbf{E}\cdot\mathbf{e}_1)\}E_{\mathrm{dc}}E_1E_2, \tag{1}$$

where E_1 and E_2 are the amplitudes of the pump waves with frequencies ω_1 and ω_2; $\mathbf{e}_1$ and $\mathbf{e}_2$ are unit polarization vectors of the corresponding waves; and, E_{dc} and $\mathbf{E}$ are the intensity and the unit vector specifying the direction of the dc electric field.

Figure 2 shows the CRS signal intensity as a function of the angle β between the polarization vector $\mathbf{e}_1$ of the pump wave with frequency ω_1 and the direction of the dc field $\mathbf{E}$, collinear with the polarization vector $\mathbf{e}_2$ of the pump wave with frequency ω_2. Since $\chi^{(3)}_{1212}=\chi^{(3)}_{1221}$ for the completely symmetric vibrations, measurements at the maximum and minimum of the dependences presented make it possible to determine the ratio of the components of the nonlinear susceptibility tensor: $\chi^{(3)}_{1122}/\chi^{(3)}_{1212}=17.3\pm2.1$. This

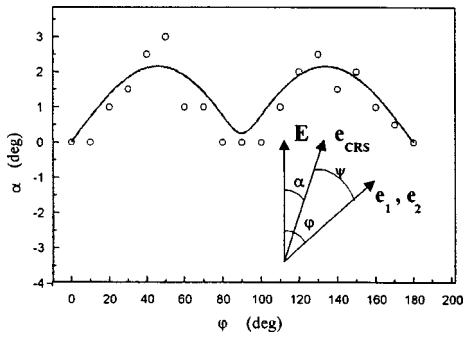

FIG. 3. Modulus of the angle α between the polarization vector $\mathbf{e}_{\mathrm{CRS}}$ of the CRS signal and the direction of the dc electric field **E** versus the angle φ between the direction of the dc field and the collinear biharmonic pump vectors $\mathbf{e}_1$ and $\mathbf{e}_2$. Dots — experimental data. Solid curve — calculation using Eq. (1).

result agrees well with the values of the invariants of the Raman scattering tensor — the average polarizability $a=1.04\times10^{-25}$ and anisotropy $g=0.79\times10^{-25}$, measured according to radiation absorption at the same transition in H_2 in the presence of an external electric field.[8]

Taking into account the polarization properties of the CRS signal, one can determine the orientation of the dc electric field can be in the general case by a procedure based on measurement of the angle ψ between the collinear polarization vectors of the biharmonic pump (the light waves with frequencies ω_1 and ω_2) and the polarization vector $\mathbf{e}_{\mathrm{CRS}}$ of the CRS signal (inset in Fig. 3). As a result of the rotation of the pair of collinear vectors $\mathbf{e}_1$ and $\mathbf{e}_2$ in a certain plane, the angle ψ vanishes when the dc electric field vectors fall on this plane. The exact direction of the dc field can be reconstructed by searching for the maximum of the CRS signal. For the investigated transition in the hydrogen molecule, the general procedure described above for determining the direction of the dc electric field can be simplified by taking into account the relation obtained between the components of the nonlinear optical susceptibility tensor (the relation determining the polarization properties of the CRS signal for this transition). In this case, for collinear vectors $\mathbf{e}_1$ and $\mathbf{e}_2$ the direction of the polarization vector of the CRS signal, according to Eq. (1), is essentially the same, for any angle φ, as the direction of the component of the dc field perpendicular to the wave vectors of the pump waves. The dependence of the modulus of the angle α between the polarization vector of the CRS signal and the direction of the dc electric field on the angle φ between the direction of the dc field and the collinear biharmonic pump vectors $\mathbf{e}_1$ and $\mathbf{e}_2$ is shown in Fig. 3. The dots are the experimental data. The solid curve was calculated using Eq. (1).

Thus the investigation of the polarization properties of the CRS signal in molecular hydrogen in a dc electric field has made it possible to determine the ratio of the components of the cubic nonlinear optical susceptibility tensor and the invariants of the Raman scattering tensor of the $Q(1)$ transition of molecular hydrogen ($\nu=0$, $J=1\rightarrow\nu=1$, $J=1$) in the electronic ground state $X^1\Sigma_g^+$. The CRS polarization technique makes it possible to realize a convenient scheme for local contactless measurement of dc electric fields in molecular gases, which is promising for solving problems of diagnostics of a

gas-discharge plasma, including measurement of plasma fields and the parameters associated with them.

This work was performed in accordance with the ''Integration'' program at the Center for Science Education ''Fundamental Optics and Spectroscopy,'' and it was partially supported by a Russian Fund for Fundamental Research Grant No. 99-02-16339 and the ''Fundamental Spectroscopy'' program of the Ministry of Science of the Russian Federation. The participation of D. A. Akimov in this work was partially supported by a Grant from the International Soros Science Education Program (ISSEP).

[1] S. A. Akhmanov and N. I. Koroteev, *Methods of Nonlinear Optics and Light Scattering Spectroscopy* (Nauka, Moscow, 1981).
[2] S. A. J. Druet and J.-P. E. Taran, Prog. Quantum Electron. **7**, 1 (1981).
[3] A. C. Eckbreth, *Laser Diagnostics for Combustion Temperature and Species* (Abacus, Cambridge, 1988).
[4] A. M. Zheltikov and N. I. Koroteev, Usp. Fiz. Nauk **169**, 385 (1999).
[5] V. P. Gavrilenko, E. B. Kupriyanova, D. P. Okolokulak *et al.*, JETP Lett. **56**, 1 (1992).
[6] O. A. Evsin, E. B. Kupriyanova, V. N. Ochkin *et al.*, Kvantovaya Élektron. (Moscow) **23**, 295 (1995).
[7] A. M. Zheltikov and N. I. Koroteev, Kvantovaya Élektron. (Moscow) **26**, 73 (1999).
[8] J. V. Foltz, D. H. Rank, and T. A. Wiggins, J. Mol. Spectrosc. **21**, 203 (1966).

Translated by M. E. Alferieff

Microscopic description of the kinetics of a martensitic transition in real crystals: bcc–hcp transition in Zr

Yu. N. Gornostyrev, M. I. Katsnel'son, and A. R. Kuznetsov
Institute of Metal Physics, Ural Branch of the Russian Academy of Sciences, 620219 Ekaterinburg, Russia

A. V. Trefilov
Kurchatov Institute Russian Science Center, 123182 Moscow, Russia

(Submitted 12 July 1999)
Pis'ma Zh. Éksp. Teor. Fiz. **70**, No. 6, 376–380 (25 September 1999)

The kinetics of the bcc–hcp transition in Zr in the presence of dislocations is investigated by numerical simulation methods. It is shown that the transition occurs in a nondiffusional (at a velocity of the order of the speed of sound) in two stages: relatively long development of instability of long-wavelength acoustic phonons and a fast stage of instability of short-wavelength phonons. The elastic stresses near a dislocation make it possible for these instabilities to develop at much lower temperatures than in an ideal crystal. © *1999 American Institute of Physics.* [S0021-3640(99)00318-7]

PACS numbers: 81.30.Kf, 64.70.Kb, 61.72.Lk

The description of the kinetics of first-order phase transitions is classic, but the statistical physics problem is still topical.[1–3] The kinetics of transitions such as the liquid–gas transition[4] and ordering in alloys,[3] which occur in a diffusional way, have now been investigated in detail using phenomenological approaches. At the same time, the so-called martensitic phase transitions, which occur in a nondiffusional way, at velocities close to the speed of sound, are well-known.[5] Even though these are first-order phase transitions, they are usually accompanied by a quite wide region of pretransitional anomalies, for example, softening of the phonon spectra.[6,7] These features make martensitic transitions close to second-order transitions. Numerous attempts to describe the kinetics of martensitic transitions on the basis of a phenomenological approach[8–10] have left a number of fundamental questions unanswered. Judging from everything, the currently known scenarios of homogeneous nucleation of a new phase do not agree with the experimental data, and crystal lattice defects should play a decisive role in the kinetics.[10,11] In the last few years, attempts have been made to study the kinetics of martensitic transitions on the basis of a microscopic approach (the molecular dynamics method).[11,12] However, in this methods the defects are either completely neglected[12] or else quite artificial models of the sources of internal stresses,[11] which do not refelect the real situation, are introduced to take these stresses into account. In the present letter we propose a microscopic description of the kinetics of a martensitic transition in zirconium in the presence of typical defects, such as dislocations.

The interatomic interaction was described by multiparticle potentials,[13] which satisfactorily reproduce the elastic properties, the phonon spectrum, and the phase diagram (temperature–pressure) of Zr. Numerical simulation of the bcc–hcp transformation by the molecular dynamics method was performed in the presence of edge dislocations with Burgers vectors $\langle 100\rangle$ and $1/2\langle 111\rangle$ (such dislocations are typical for a bcc lattice). We note that dislocations with Burgers vectors $\langle 100\rangle$ are inherited in a bcc–hcp transition, remaining whole (unsplit),[14] while dislocations with Burgers vectors $1/2\langle 111\rangle$ split into partial dislocations, forming a stacking fault band, complicating the picture of the transition. Here we shall present in detail the results for dislocations of the first type. A rectangular crystallite in the form of a slab with a thickness of 12 atomic planes along the Z axis (the Z axis is directed along the dislocation line and the X axis is directed parallel to the Burgers vector) contained about 10,000 atoms; periodic boundary conditions were used in all three directions. To ensure periodicity in the X and Y directions, a pair of dislocations of opposite sign (a dipole) was introduced into the crystallite. These dislocations were repeated as dislocations of the images outside the crystallite boundaries also. The average kinetic energy of the atoms was used to check the constancy of the temperature.

A bcc structure was prescribed as the initial configuration in the crystallite. In Zr it is metastable at temperatures $T<1136$ K, and an hcp lattice corresponds to the true minimum of the free energy. This feature can be correctly described on the basis of the model which we employed for the interatomic interactions. Despite this, the initial configuration remained stable at $T=300$ K throughout the entire, quite long, simulation time. Specifically, the crystallite remains in a bcc phase after 10^5 steps (one step corresponds to 10^{-15} s), while in the presence of dislocations the transition is completed after 10^4 steps. This is explained by the quite high barrier separating the bcc and hcp phases (see, for example, the form of the potential relief for a bcc–hcp transition according to the microscopic calculations for barium;[15] unfortunately, the corresponding calculations have not been performed for zirconium, but the form of the relief in these cases should be qualitatively similar). Therefore dislocations initiate a rapid transformation of the supercooled metastable bcc phase.

Figure 1 shows the stages of the nucleation of the bands of the hcp phase from the bcc phase near dislocations at $T=300$ K. According to generally accepted ideas, the crystal geometry of a bcc–hcp transition is determined by a Burgers deformation entailing a long-wavelength shear strain and a short-wavelength deformation (the mode N_4').[15,16] The computational results make it possible to describe the development of this transition in time. A stage in which an instability of long-wavelength (acoustic) transverse phonons with vector $\mathbf{k}\parallel\langle 110\rangle$ develops is observed first. Then the initially sinusoidal oscillations (Fig. 1a) transform into a sequence of kinklike excitations with quite sharp boundaries (Figs. 1b and 1c). Next, after a series of domain boundaries has formed, a short-wavelength instability, which determines the specifically hcp character of the new phase (Fig. 1c), develops in a very short time. This is clearly seen from the computational results for the radial distribution function of the atoms (Fig. 2), where the peaks corresponding to the position of the first, second, and third neighbors in the bcc lattice vanish, and similar peaks for the hcp structure appear.

The transition picture described above is not dictated by dislocations. Our calculations show that in the absence of dislocations the transition occurs according to a similar

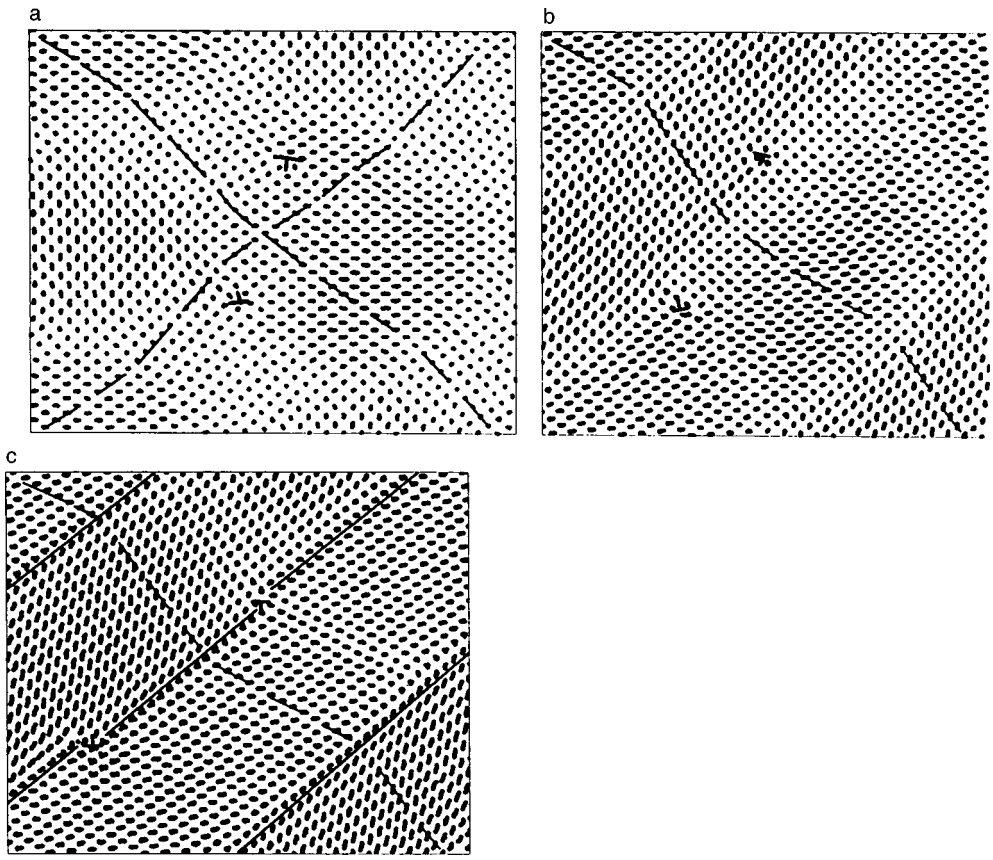

FIG. 1. Projection on the (001) plane of the crystallite under study at different stages of the bcc–hcp transition at 300 K after 18000 (a), 28000 (b), and 43000 (c) steps. The symbol $\perp$ marks dislocations with Burgers vectors $\pm\langle 100\rangle$. During relaxation, dislocations move away from the initial dipole configuration, stopping on twin boundaries (Fig. 1c). The dashed lines show the evolution of the initially sinusoidal waves, corresponding to the soft mode, into a soliton lattice (system of twins).

scenario and over comparable times if the temperature is increased to 1000 K. It should be underscored that nucleation of a new phase starts not with the appearance of individual nuclei[8] but rather with the development of a phonon instability, as proposed in Ref. 6. The prerequisites for the appearance of this instability seem to be the presence of a soft branch of transverse phonons in the $\langle 110\rangle$ direction and strong anharmonicities of the potential for this branch in bcc Zr.[17] As a result, contrary to the existing general ideas about the kinetics of first-order phase transitions,[1,2] the new phase can arise immediately in the form of an ordered system of twins, and the stage of growth of a solitary nucleus does not occur at all. From the standpoint of the soliton approach in the theory of martensitic transitions,[9] the formation of such a system of twins can be naturally described as the appearance of a soliton lattice as a result of the instability of small-amplitude phonons with respect to self-modulation (see Ref. 6). In other words, this can be related to minimization of the elastic energy of the system by formation of twins.[5] The relation between the soliton approach and these considerations has been discussed in

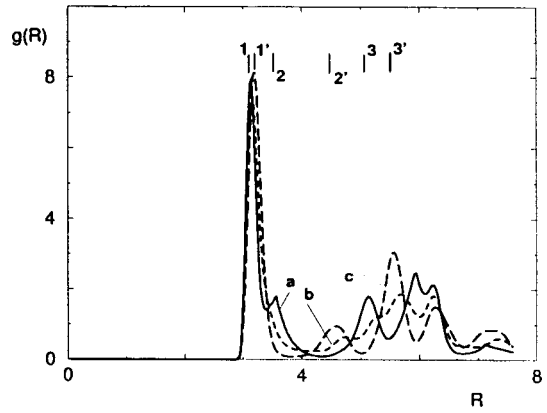

FIG. 2. Evolution of the radial distribution function in the process of a bcc–hcp transition. The curves a, b, and c correspond to the transformation stages shown in Figs. 1a, 1b, 1c, respectively. The positions of the first-, second-, and third-nearest neighbors in the bcc structure are denoted by 1, 2, and 3 and the positions in the hcp structure are denoted by $1'$, $2'$, and $3'$, respectively.

detail in Ref. 18. It should be underscored that although in our calculations the entire crystallite transformed into the hcp phase (which is due to its relatively small size), the choice of periodic boundary conditions simulates to some degree the ''compressed'' state of the precipitates of the new phase in the bcc matrix during a real martensitic transformation. A procedure that simulates constant-pressure conditions could give a different picture of the transition.[19] Such a procedure corresponds to an idealized picture of a crystal with no internal stresses. As to the generality of our results, it can be supposed that at least the initial stages of development of the instability of the acoustic phonons are universal for a transition from a bcc to any close-packed structure, since these transitions are all due to the ''softness'' of the bcc lattice with respect to the shear strain associated with a $\langle 110 \rangle$ phonon with polarization vector $\langle \bar{1}10 \rangle$.[7] At the same time, the final stage of the development of instability, associated with an N_4' phonon, is specific to a transition to an hcp structure. It would be interesting to check these considerations by modeling a transition for other metals.

In conclusion, we shall correlate our results with various phenomenological ideas about the role of dislocations and other defects in the kinetics of martensitic transitions.[10,20] In Ref. 10 the important role of ''soft'' regions near defects, where the local shear modulus is much smaller than in an ideal crystal or even negative, is underscored. In Ref. 20, the change in the energy difference between two phases, i.e., the decrease in the height of the barrier near a dislocation, as a result of elastic stresses was considered to be the main factor. The first point of view undoubtedly agrees better with the ''wave'' nature, demonstrated here, of a martensitic transition (phonon instability). Our computational results show that the instability of acoustic phonons, which ultimately results in the formation of a system of twin boundaries, develops first near a dislocation in a region making an angle of 45° with the Burgers vector. This region corresponds to the maximum shear strain and a small dilatation.[21]

We thank our colleagues J. Morris and D. Turner at the Ames Laboratory of the US Department of Energy for providing the molecular dynamics programs and the inter-

atomic interaction potentials for zirconium. This work was supported by the Russian Fund for Fundamental Research (Project No. 98-02-16219).

[1] Ya. B. Zel'dovich, Zh. Éksp. Teor. Fiz. **12**, 525 (1942).
[2] J. W. Cahn, Acta Metall. **5**, 168 (1957).
[3] V. G. Vaks, JETP Lett. **63**, 471 (1996).
[4] K. Binder and M. Kalos, in *Monte Carlo Methods in Statistical Physics*, edited by K. Binder (Springer-Verlag, New York, 1979) [Russian translation, Mir, Moscow, 1989].
[5] G. V. Kurdyumov, in *Problems of Modern Physics*, edited by A. P. Aleksandrov (Nauka, Moscow, 1980) p. 396.
[6] M. I. Katsnel'son and A. V. Trefilov, Fiz. Met. Metalloved. **64**, 629 (1987).
[7] M. I. Katsnelson, I. I. Naumov, and A. V. Trefilov, Phase Transit. **49**, 143 (1994).
[8] A. L. Roĭtburd and A. G. Khachaturyan, Fiz. Met. Metalloved. **30**, 1189 (1970).
[9] J. A. Krumhansl, Phase Transitions B **65**, 109 (1998).
[10] G. Guenin and P. F. Gobin, Metall. Trans. A **13**, 1127 (1982).
[11] P. C. Clapp, Physica D **66**, 26 (1993).
[12] P. Entel, K. Kadau, R. Meyer *et al.*, Phase Transitions B **65**, 79 (1998); R. Meyer and P. Entel, Comput. Mater. Sci. **10**, 10 (1998).
[13] J. R. Morris, Y. Y. Ye, K. M. Ho *et al.*, Philos. Mag. A **72**, 751 (1995).
[14] G. É. Braĭnin and V. A. Likhachev, Metallofizika (Kiev) **4**, 50 (1982).
[15] Y. Chen, K. M. Ho, and B. N. Harmon, Phys. Rev. B **37**, 283 (1988).
[16] W. G. Burgers, Physica (Amsterdam) **1**, 561 (1934).
[17] W. Petry, Phase Transitions B **31**, 119 (1991); Yu. N. Gornostyrev, M. I. Katsnelson, A. V. Trefilov *et al.*, Phys. Rev. B **54**, 3286 (1996).
[18] B. Horovitz, J. L. Murray, and J. A. Krumhansl, Phys. Rev. B **18**, 3549 (1978).
[19] B. L. Zhang, C. Z. Wang, K. M. Ho *et al.*, Phys. Rev. Lett. **74**, 1375 (1995).
[20] I. M. Dubrovskiĭ and M. A. Krivoglaz, Zh. Éksp. Teor. Fiz. **77**, 1017 (1979) [Sov. Phys. JETP **50**, 512 (1979)].
[21] J. P. Hirth and J. Lothe, *Theory of Dislocations* (McGraw-Hill, New York, 1967) [Russian translation, Atomizdat, Moscow, 1972].

Translated by M. E. Alferieff

Long-range influence of weak optical irradiation of silicon

D. I. Tetel'baum,*) V. A. Panteleev, and M. V. Gutkin
Scientific-Research Physicotechnical Institute, N. I. Lobachevski Nizhniĭ Novgorod State University, 603600 Nizhniĭ Novogorod, Russia

(Submitted 16 July 1999)
Pis'ma Zh. Éksp. Teor. Fiz. **70**, No. 6, 381–385 (25 September 1999)

We report a new effect, observed experimentally in silicon under irradiation with visible-range light with a power density of 0.2–1.5 W/cm^2 for 8 s. The effect consists in an increase of microhardness on the side opposite to the irradiated side and is not purely thermal in character. After irradiation, the changes decrease exponentially with time with an activation energy of 0.75 ± 0.05 eV, a value which is characteristic for the migration and reorientation of one of the types of intrinsic interstitial atoms. A qualitative explanation is given for the effect on the basis of a model previously proposed for the case of long-range influence of ion irradiation. © *1999 American Institute of Physics.* [S0021-3640(99)00418-1]

PACS numbers: 61.82.Fk, 61.80.Ba, 61.80.Jh, 81.40.Wx

In the present work we have observed a new effect, which lies at the interface between two groups of previously studied phenomena: long-range influence (LRI) of the irradiation of solids by charged particles[1–3] and defect formation in semiconductors under photon irradiation.[4,5] LRI was first observed for ion irradiation of semiconductors and metals. The crux of this effect consists in a change in the structure and properties at anomalously large depths, hundreds and thousands of times greater than the ion ranges. Later it was found that a similar effect also occurs for other types of influences acting on the surface layer of solids, such as electron irradiation, polishing, plasma and chemical etching, rubbing, and so on. In some cases the effect can be explained on the basis of conventional ideas based on the existence of strong nonstationary heating of a subsurface layer and accompanying phenomena, e.g., nonuniform deformation and the excitation of shock waves. In other cases, however, the heating is clearly insufficient for these phenomena to appear. This latter category includes the effects investigated in our previous studies: a low-dose long-range influence (LD-LRI) in metals,[3] and LRI in silicon.[6–9] We have proposed[1–3,6–8] a model of LRI based on the idea of the generation of elastic waves in the zone of energy release and their interaction with extended defects. The role of the latter follows from the fact that the LD-LRI and LRI in silicon have been observed only in materials containing a high density of extended defects — grain boundaries, subgrains, dislocation loops, stacking faults, and so on.

An important characteristic feature of LD-LRI is the absence of any correlation with the mechanism of direct transfer of energy from the particle beam to the solid — this mechanism manifested almost identically under irradiation with heavy or light ions or

with electrons, while nuclear (elastic) stopping dominates in the first case, electronic stopping dominates in the second case, and in the third case all of the energy of the incident particles is initially transferred to the electronic subsystem. On the basis of this fact it was natural to consider a different group of phenomena — subthreshold defect formation in semiconductors. There is extensive literature on this question (see Refs. 4 and 5), concerning irradiation by electrons, hard (vacuum) ultraviolet radiation, x rays, and light (photochemical reactions[10]). Numerous experimental data on the stimulated diffusion of impurities and the change in the electric and optical properties are discussed; various models of subthreshold defects are presented. These works border on the investigation of the so-called photomechanical effect — the change induced in the microhardness of semiconductors and dielectrics by illumination directly during indentation by an indenter.[11] It has also been reported that changes in the mechanical properties are observed when metal films and foils are illuminated by vacuum ultraviolet light.[12] Since the penetration depth of vacuum ultraviolet light in metals is very short, such changes can be explained only by LRI.

In Ref. 13 we reported a photomechanical memory effect in metals. It was established that the microhardness of Permalloy foils changes on the side opposite to the irradiated side under irradiation with a 0.95 μm laser. The effect was not due to heating and was explained on the basis of a model which we used previously for the case of LD-LRI under ion irradiation.

On this basis it could be conjectured that a long-range influence of relatively weak light fluxes on the properties of semiconductors is in principle possible and is not limited by purely electronic processes, but rather it can be caused by structural changes. However, no indications of this for elementary covalent semiconductors (such as silicon or III–V compounds) could be found in the literature, with the exception of data on the light-stimulated diffusion of certain impurities (Au and others).[4,5]

In the present work we used 0.5 mm thick silicon wafers subjected to thermal oxidation in a ''dry–wet–dry'' cycle. (It was established previously[7] that in oxidized silicon, where the surface layers are enriched with oxidizing stacking faults, the LRI is strongest under ion irradiation.) Prior to oxidation the wafers were polished on one side mechanically and on the other side by a chemical-mechanical method followed by dynamic etching. The oxide layers were removed prior to irradiation. The mechanically polished side was irradiated for $\tau = 8$ s by light from a 300 W halogen lamp with light flux intensity $I = 0.2 - 1.5\,\mathrm{W/cm^2}$. After irradiation from the opposite side, measurements of the microhardness H under a 200 g load were performed. The microhardness method was chosen because it was a test method for investigating LRI in solids. Changes in H signal the presence of not only electronic but also structural changes, which should be investigated later by more precise methods. It was found beforehand that for all practical purposes the changes in H do not increase for $\tau > 8$ s. A 20 g load was close to optimal from the standpoint of compromising between the sensitivity of H to irradiation and minimization of the experimental error. The error in the measurements of H with allowance for the statistics did not exceed 3% at a 0.95 probability level. The time between illumination and measurements of H was (except in the relaxation experiments) of the order of 10–100 min. Most experiments were performed using a ZhS-16 light filter, which absorbs radiation with $\lambda \leqslant 0.5$ μm. This was done in order to cut off any possible effects which are characteristic for high photon energies (these are described in Refs. 4

and 5). To decrease the heating of the samples with a light beam, the samples were mounted on a massive metal flange; the temperature did not exceed 50°C. To improve heat removal, some samples were mounted on the flange through a layer of vacuum grease, in which case there was virtually no heating.

The experiments showed that irradiation increases H, the increase reaching 20%. Before discussing this phenomenon from the standpoint of the mechanisms which we proposed previously for ion irradiation, the possibility of alternative explanations must be considered.

1. *Effect of purely thermal action of a light beam.* As a check, we performed annealing in a furnace at 130°C, i.e., at a temperature known to be much higher than the temperature reached under the beam. The value of H did not change within the limits of error. The fact that the effect did not occur for samples in which a ~ 20 μm layer enriched with stacking faults was removed from the irradiated side beforehand confirmed the athermal character of the effect. The influence of this layer is discussed below. In addition, the effect did not vanish when the samples were mounted with vacuum grease.

2. *Influence of light penetration to the back side.* In our case this factor can also be ruled out. Only photons with energy $E_{ph} \leqslant E_g$, where E_g is the band gap, penetrated through the thickness of the sample. However, when a silicon filter was used, no changes were observed in H on the sample side turned toward the filter (or on the opposite side). At the same time, the effect did not vanish when filters transmitting light with photon energy $E_{ph} \geqslant 2$ eV, for which $k^{-1} < 3$ μm (k is the absorption coefficient), were used.

3. *Influence of excess minority carriers on the back side.* This factor is also unimportant, since the diffusion length of the minority carriers was ~ 20 μm, i.e., more than an order of magnitude smaller than the thickness of the samples. Moreover, thinning the samples by a factor of 2 did not intensify the effect but rather weakened it (because the layers enriched with stacking faults were etched off).

Thus, the effect is clearly due to the fact that photons exciting electron–hole pairs are absorbed in the sample. Moreover, extended defects — oxidizing stacking faults — play an important role. Comparing these facts with previously obtained results on LRI under ion irradiation,[1–3,6–8], we can infer with a high degree of assurance that this effect is based on the same mechanism, specifically, the generation of elastic waves and their interaction with a system of defects in the presence of positive feedback between the elastic waves and the system of defects. For ion irradiation the source of elastic waves is reactions between radiation defects and (or) thermal peaks.[1] For irradiation with light, elastic waves arise when the excited carriers recombine via recombination centers (point defects). In accordance with the Lang model,[4,5] the energy released in the process is transferred to a defect, increasing the oscillation amplitude of the defect. Subsequently, chain processes with the participation of extended defects come into play. These processes ultimately result in energy transfer to defects near the back side of the plate and a concomitant change in H. This mechanism has been described in greater detail in Refs. 1 and 8 for ion irradiation, and the details of the mechanism for photon irradiation will be presented separately (see also Ref. 13).

Figure 1 shows the dependence of the magnitude of the effect (the relative increase in H) on the power density, regulated by the source–sample distance. The characteristic nonlinearity of the dependence and the presence of a threshold power have been observed

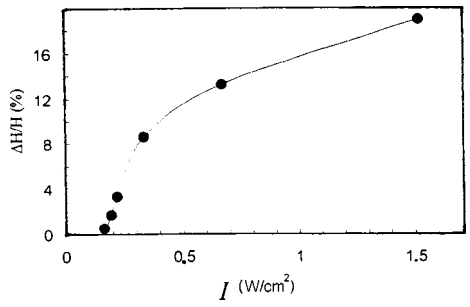

FIG. 1. Relative change in the microhardness versus the power density under irradiation with light through a ZhS-16 light filter.

previously for ion irradiation of silicon,[6] and these dependences are quantitatively very close, once again confirming that both effects are of the same nature.

In contrast to the case of ion irradiation, here the change in H is unstable in time and relaxes exponentially over several days, i.e., relaxation occurs as a result of a monomolecular reaction (Fig. 2). The activation energy of the process was found by accelerated relaxation at temperature 60–100°C to be 0.75 ± 0.05 eV. This is close to the migration and reorientation energy of one of the types of intrinsic interstitial silicon atoms.[14] It can be inferred that the reactions involving the participation of intrinsic interstitial atoms limit the structural relaxation process after irradiation near the surface — at the boundary with the native oxide.

Let us discuss the effect observed here from the standpoint of comparison with the data obtained by other authors. Subthreshold defects in semiconductors have been investigated predominantly for irradiation by electrons and x rays. For InSb and Ge these effects have been explained on the basis of an impurity–ionization mechanism, which, however, is ineffective for Si.[5] For the latter, the subthreshold mechanism of defect formation is attributed to ionization of the K shell, which is ruled out for irradiation with light. Dissociative (photochemical) mechanisms, discussed for complex semiconductors,[5] are also inapplicable to Si. The defect formation mechanism proposed by Sheĭnkman[10] is also applicable in its general form for elementary semiconductors, but it does not explain the long-range influence. The situations studied in works on the effect of light on impurity diffusion in silicon are substantially different from our case. Therefore we are indeed dealing with a new effect.

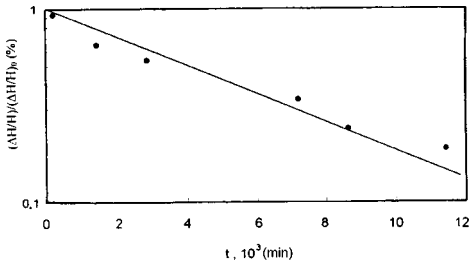

FIG. 2. Change in the microhardness at room temperature after irradiation with light with power density 1.5 W/cm^2.

If long-range changes in the structure and properties exist in semiconductors irradiated with relatively weak light fluxes, then this is important for studying a variety of electric and photoelectric phenomena in semiconductor materials and devices. Such phenomena could be one reason for the interaction of functioning structures in matrices of transistors, avalanche diodes, and so on. They could influence the degradation and noise properties of devices (injection of charge carriers can be realized not only by light but also by an electric field) and also on the properties of low-dimensional structures. The criterion of a high density of extended defects is not too strong a constraint — it holds in a wide class of semiconductor devices, including many low-dimensional structures (quantum wells and quantum dots).

Let us conclude by offering some reasons why the effect has not been observed earlier.

1. It can be observed only when the following conditions are satisfied simultaneously: adequate power density; presence of specific extended defects, for example, stacking faults; limited time interval between the action and the measurement (on account of relaxation); definite duration of the action.

2. Ordinarily, the phenomena occurring on the nonworking side of a wafer were of interest from the standpoint of impurity gettering, while the possibility of the interaction of structural elements on the working side have been considered only in their purely electronic or photoelectronic aspects or from the standpoint of static fields of elastic stresses. Our investigation of the effect was stimulated by the study of LRI under ion irradiation.

*)e-mail: ett@phys.unn.runnet.ru

[1] P. V. Pavlov, Yu. A. Semin, V. D. Skupov *et al.*, Fiz. Tekh. Poluprovodn. **20,** 503 (1986) [Sov. Phys. Semicond. **20**, 315 (1986)].
[2] P. V. Pavlov, D. I. Tetelbaum, V. D. Skupov *et al.*, Phys. Status Solidi A **94**, 395 (1986).
[3] D. I. Tetelbaum, E. V. Kurilchik, and N. D. Latisheva, Nucl. Instrum. Methods Phys. Res. B **127/128**, 153 (1997).
[4] M. I. Klinger, Ch. B. Lushchik, T. V. Mashovets *et al.*, Usp. Fiz. Nauk **147,** 523 (1985) [Sov. Phys. Usp. **28**, 994 (1985)].
[5] V. S. Vavilov, A. E. Kiv, and O. R. Niyazova, *Mechanisms of Formation and Migration of Defects in Semiconductors* (Nauka, Moscow, 1981).
[6] P. V. Pavlov, D. I. Tetel'baum, E. V. Kuril'chik *et al.*, Vysokochistye Veshchestva **4**, 26 (1993).
[7] V. D. Skupov, D. I. Tetel'baum, and V. G. Shengurov, Pis'ma Zh. Tekh. Fiz. **15**(22), 44 (1989) [Sov. Tech. Phys. Lett. **15**, 890 (1989)].
[8] Yu. A. Semin, V. D. Skupov, and D. I. Tetel'baum, Pis'ma Zh. Tekh. Fiz. **14,** 273 (1988) [Sov. Tech. Phys. Lett. **14**, 121 (1988)].
[9] Yu. A. Aleshenko, E. A. Bobrova, V. S. Vavilov *et al.*, Radiat. Eff. Defects Solids **25**, 323 (1993).
[10] M. K. Sheĭnkman, JETP Lett. **38**, 330 (1983).
[11] N. N. Novikov, Ukr. Fiz. Zh. (Russ. Ed.) **17**, 724 (1972).
[12] A. A. Koz'ma, S. V. Malykhin, O. V. Sobol' *et al.*, Fiz. Met. Metalloved. **7**, 168 (1991).
[13] D. I. Tetel'baum, A. Yu. Azov, A. A. Trofimov *et al.*, Pis'ma Zh. Tekh. Fiz. **24,** 9 (1998) [Tech. Phys. Lett. **24**, 910 (1998)].
[14] A. Zeeger, H. Föll, and W. Frank, in *Radiation Effects in Semiconductors, 1976*, edited by N. R. Urli and J. W. Corbett (The Institute of Physics, Conference Series Number 31, London, 1977) [Russian translation, Mir, Moscow, 1979].

Translated by M. E. Alferieff

Antipolarization effect in quantum wells in a strong external alternating field

V. A. Burdov*)
N. I. Lobachevski Nizhniĭ Novgorod State University, 603600 Nizhniĭ Novgorod, Russia

(Submitted 8 October 1998; resubmitted 24 May 1999)
Pis'ma Zh. Éksp. Teor. Fiz. **70**, No. 6, 386–391 (25 September 1999)

It is shown that when a strong ac electric field acts on an electron in a double quantum well, the dipole moment is an almost periodic function of the dc voltage applied to the structure. An antipolarization effect — the structure is polarized in a direction opposite to the external field — appears during one half of the period. © *1999 American Institute of Physics.* [S0021-3640(99)00518-6]

PACS numbers: 73.20.Dx

Processes associated with the interaction of powerful laser radiation with the electronic subsystem of various quantum heterostructures, specifically, heterostructures with a double quantum well, have been increasingly studied in recent years. Phenomena such as the dynamic localization of the electronic wave function in one of the wells by a strong ac field,[1–3] low-frequency generation of electromagnetic radiation,[4,5] and absolute negative resistance,[6,7] have been observed. In the present letter a completely new effect is reported — an antipolarization effect. The crux of this effect is that in the presence of a strong ac perturbation a quantum system becomes polarized in a direction opposite to an external dc electric field.

We shall describe the symmetric double quantum well by a two-level model ($E_{0,1} = \pm \hbar\Delta/2$) with the wave functions $\chi_0(x)$ and $\chi_1(x)$, which are symmetric and antisymmetric, respectively, and for which the quantity $\chi_0^2(x) - \chi_1^2(x)$ is negligibly small along the entire x axis. We suppose that the external field consists of two parts — a dc component $\overline{V}(x)$ (its average value) and an ac component $\tilde{V}(x,t)$ with frequency ω, and we assume that the matrix elements $\overline{V}_{01}$ and $\tilde{V}_{01}(t)$ calculated in the dipole approximation are much greater than the transition energy $\hbar\Delta$.

The objective of the present work is to calculate the electronic dipole moment in a strong periodic external field $\tilde{V}(x,t)$ and to analyze the dependence of the dipole moment on the dc voltage $-\overline{V}(x)/e$ ($-e$ is the electron charge) applied to the system.

In a strong periodic external field the stationary states with definite energy are effectively replaced by states with definite quasienergy.[8] The wave functions of the quasienergy states then have the Bloch form

$$U(x,\tau) = \Phi(x,\tau)e^{-i\nu\tau}, \tag{1}$$

where $\tau=\omega t$, the number ν is a dimensionless quasienergy calculated in units of $\hbar\omega$, and the quasienergy function $\Phi(x,\tau)$ is periodic in τ with period 2π.

We shall seek the function $\Phi(x,\tau)$ in the form of an expansion in an orthonormal basis of functions $\Psi_{\pm}(x)=(\chi_0(x)\pm\chi_1(x))/\sqrt{2}$ localized in the right-hand (Ψ_+) and left-hand (Ψ_-) wells:

$$\Phi(x,\tau)=A(\tau)\exp\left\{i\left(\gamma\tau/2+\int \nu(\tau)d\tau\right)\right\}\Psi_-(x)+B(\tau)$$
$$\times\exp\left\{-i\left(\gamma\tau/2+\int \nu(\tau)d\tau\right)\right\}\Psi_+(x), \tag{2}$$

where $\gamma=2\overline{V}_{01}/\hbar\omega$, $\nu(\tau)=\tilde{V}_{01}/\hbar\omega$, and $A(\tau)$ and $B(\tau)$ are functions of time to be determined. Substituting the wave function (1) with $\Phi(x,\tau)$ in the form (2) into the Schrödinger equation, we obtain the following equations for $A(\tau)$ and $B(\tau)$:

$$i\frac{dA}{d\tau}+\nu A=-\frac{B}{2}\sum_{n=-\infty}^{\infty}\mu_n e^{-i\psi_n}e^{-i(\gamma-n)\tau},$$

$$i\frac{dB}{d\tau}+\nu B=-\frac{A}{2}\sum_{n=-\infty}^{\infty}\mu_n e^{i\psi_n}e^{i(\gamma-n)\tau}, \tag{3}$$

where

$$\mu_n\exp\{i\psi_n\}=\frac{\Delta}{2\pi\omega}\int_0^{2\pi}d\tau\exp\left\{i\left(n\tau+2\int \nu(\tau)d\tau\right)\right\} \tag{4}$$

is Δ/ω times the amplitude of the nth Fourier harmonic of the function $\exp\{2i\int\nu(\tau)d\tau\}$ (i.e., $\mu_n\omega/\Delta$ is the modulus of the harmonic).

The coefficients (4) of the Fourier expansion, by definition, do not depend on the external dc field but are functions of the amplitude and frequency of the variable component of the external field. In addition, since the amplitude of the variable perturbation is assumed to be large, the integrand in Eq. (4) is rapidly oscillating, and therefore the value of the integral is small. For example, for a purely harmonic perturbation $\tilde{V}_{01}(t)=W\cos\omega t$, the coefficients μ_n are equal to $J_n(2W/\hbar\omega)\Delta/\omega$, where $J_n(x)$ are Bessel functions of argument x. If $W/\hbar\omega\gg 1$, the coefficients μ_n will be small for any n. For a nonharmonic but, as before, periodic perturbation, the integral in Eq. (4) can be calculated by the method of stationary phase, as was done in Ref. 9. The conclusion that μ_n is small remains valid, making it possible to solve the system (3) analytically.

Of greatest interest is the solution in the so-called resonance case, when the transition frequency between energy levels is a multiple of the frequency of the external field. When the dc component of the external field is large, as we assumed initially, the transition frequency is $2\overline{V}_{01}/\hbar$, and therefore the resonance condition can be expressed as

$$\gamma=n,\quad n=1,2,3,\ldots \tag{5}$$

Generally speaking, the solution obtained in the resonance approximation holds only in a narrow range $|\gamma-n|\ll 1$ and cannot be extended to the entire γ axis. However, it will be

shown below that when the coefficients μ_n are small, $\mu_n \ll |\gamma - n| \ll 1$, the solutions obtained will be entirely adequate at least for a qualitative understanding of the effect described here.

Let us obtain the solution of Eqs. (3) near an arbitrary lth resonance. For this, as usual, we drop in Eq. (3) all ''fast'' harmonics, retaining in the sums only the ''slow'' term with $n=l$. Then the system (3) can be easily solved, giving two quasienergy functions:

$$\Phi_{\pm}(x,\tau) = \Psi_{\pm}(x)\sqrt{\frac{1}{2}+\frac{\delta}{2\eta}}\exp\{\mp i\varphi_l(\tau)\} \mp \Psi_{\mp}(x)\sqrt{\frac{1}{2}-\frac{\delta}{2\eta}}\exp\{\pm i(\varphi_l(\tau)-\psi_l)\}, \tag{6}$$

corresponding to two values of the quasienergy

$$\nu_{\pm} = \pm\frac{\eta}{2} = \pm\frac{1}{2}\sqrt{\mu_l^2+\delta^2}. \tag{7}$$

Here we have introduced the detuning from resonance $\delta = \gamma - l$ and the function $\varphi_l(\tau) = \int (\nu(\tau) + l/2)\, d\tau$.

Now it is easy to find an expression for the electronic dipole moment in quasienergy states near the lth resonance. Using for this purpose the wave functions (6), we obtain

$$D_{\pm}(\delta) = \mp e x_{01}\frac{\delta}{\sqrt{\delta^2+\mu_l^2}}, \tag{8}$$

where x_{01} is the matrix element of the coordinate operator (for definiteness we shall assume it to be positive).

In accordance with Eq. (8), the dipole moment, for example, of the ''+'' state in the region of negative values of δ far from resonance, is close to its maximum possible positive value ex_{01}. A transition through the resonance point is accompanied by an abrupt change in sign of the dipole moment, with the minimum possible value $-ex_{01}$ being rapidly approached as δ increases. To all appearances, a further increase of the distance from resonance (in the region $|\delta| \sim 1$) should not greatly influence the dynamics of the system. For this reason, the dipole moment will remain at its maximum or minimum value until the system reaches the region of the next $(l-1)$th or $(l+1)$th resonance, where once again the dipole moment vector flips abruptly.

Evidently, such flipping will always occur when the parameter γ assumes its next integer value. Then the distance between the energy levels, initially coupled with one another by a resonance l-quantum process, will change by the energy of a single quantum of the external ac field.

Therefore the dependence of the dipole moment on the parameter γ (i.e., on the external dc field) in quasienergy states is almost periodic with a ''period'' of 2. Small deviations from periodicity will be observed in a small neighborhood of the resonance point $\gamma = n$, where the dipole moment changes sign. The width of the differential of the function $D_{\pm}(\gamma)$ near resonance is determined primarily by the values of the coefficients μ_n, and since in general all coefficients μ_n are different, strict periodicity is impossible.

Therefore in one ''half period'' the direction of the dipole moment is the same as the direction of the external dc field, and in the next ''half period'' the system is polarized opposite to the field, with the dipole moment reaching its largest values in both cases. Therefore an antipolarization effect, due to the additional effect of the strong ac field on an electron, arises in one of the ''half periods'' in the system.

It is easy to understand this behavior of $D_{\pm}(\gamma)$ if the structure of the quasienergy states (6) is taken into account. For example, near the lth resonance for negative values of the parameter δ (such that $\mu_l \ll |\delta| \ll 1$) the function $\Phi_+(x,t)$ is identical (to within an unimportant exponential phase factor) to the function $\Psi_-(x)$ and is therefore completely localized in the left-hand well. Then the polarization of the system has its maximum value, and the system is almost insensitive to further decreases of δ.

As exact resonance is approached ($\delta=0$), the degree of localization of an electron in the left-hand well decreases and a portion of the wave function is transferred into the right-hand well. If the resonance condition holds exactly, the quasienergy function $\Phi_+(x,t)$ fills both wells equally. An increase of δ results in further filling of the right-hand well and emptying of the left-hand well. Finally, for $\delta \gg \mu_l$ the entire wave function is completely localized in the right-hand well, which once again gives a maximum dipole moment, but this time the moment is directed in the opposite direction.

As expression (7) shows, at resonance ($\delta=0$) the quasienergy branches approach as close as possible to one another to a value determined by the coefficient μ_l. In the zeroth approximation, corresponding to $\mu_l=0$, the quasienergy branches intersect one another, i.e., degeneracy of the quasienergy spectrum, also called a quasienergy resonance, occurs. The degeneracy is lifted when the finiteness of the coefficients μ_l is taken into account — the quasienergy levels are ''split'' and a gap of width μ_l forms between the quasienergy branches. In this case the wave functions of the quasienergy states are symmetric and antisymmetric linear combinations of the two initial, zeroth-order wave functions, just as happens for degenerate stationary states. In our case the zeroth approximation corresponds to departure from resonance — when there are two quasienergy functions which are virtually completely localized in the left-hand and right-hand wells. For this reason, for $\delta=0$ their superposition with coefficients of equal absolute magnitude will necessarily give a wave function that occupies equally the left- and right-hand wells, as can be directly verified using expression (6) with $\delta=0$. It is obvious that the dipole moment of the system should vanish at the resonance points, and that is just what expression (8) gives.

A strong ac field couples the two zero-order quasienergy states localized in different wells. For this reason a transition in the parameter δ from negative to positive values through the resonance point results in a continuous transfer of the quantum system from one quasienergy state in the zeroth approximation into the other, and this transition is accompanied by a relocation of the electronic wave packet from one well to the other.

As we have said, no substantial changes in the function $\Phi_+(x,t)$ will occur in the entire range of values of δ between two resonances until γ approaches the next resonance value $l+1$ (i.e., $\delta=1$). Here a reverse transition of the electronic wave packet will occur — from the right-hand to the left-hand well, with the successive change in the direction of the polarization vector. Evidently, each successive transition through the next reso-

nance point will be accompanied by a transfer of the wave packet from one well to the other.

The behavior of the function $\Phi_-(x,t)$ is completely opposite to that of $\Phi_+(x,t)$: When one function is localized in the left-hand well, the other is localized in the right-well, and vice versa. For this reason, the dipole moments in the + and − states differ in sign.

In the most general case the wave function of the system is a superposition of both quasienergy states and can be represented by an expansion in an orthonormalized basis of functions $U_\pm(x,\tau)$:

$$\Psi(x,\tau)=C_+U_+(x,\tau)+C_-U_-(x,\tau). \tag{9}$$

As was shown in Ref. 8, the expansion (9) in the basis of quasienergy functions, in contrast to the expansion in other bases, possesses an important property: The expansion coefficients $C_\pm$ do not depend on time and are always constant. For this reason, if a state identical to one of the quasienergy states is prepared initially (i.e., one of the coefficients in the expansion (9) is 0 and the other is 1), the system remains in the given quasienergy state with probability 1. This can be easily achieved in practice by imposing on the symmetric double quantum well first a strong dc field ($\overline{V}_{01}\gg\hbar\Delta$), which results in localization of particles in the lower level (in the lower subband) in one of the wells, and then an ac field. The intensity of the dc field and the frequency of the ac field must be chosen such that the system is far from resonance, i.e., the condition (5) is far from being satisfied. Since in the nonresonant range of values of γ the functions $U_\pm(x,\tau)$ are localized in different wells, it is obvious that the particles will ''occupy'' the quasienergy state whose wave function is localized in the well containing the particle at a given moment. Subsequently, the dc field can be varied adiabatically without causing transitions of the quantum system from one quasienergy state into another, but transferring charge from one well into another with each passage through the next resonance (5).

Taking, for estimates, the width of each well and the thickness of the barrier separating the wells to be 10 nm, the barrier height to be the same in order of magnitude as the values of $E_{0,1}$, i.e., -0.1 eV, and the carrier mass to be of the order of a tenth of the free-electron mass, we obtain the transition energy $\hbar\Delta$ to be of the order of 10^{-3} eV. To ''separate'' the energy levels substantially, increasing the transition energy severalfold or even by an order of magnitude, will require dc fields $\sim 10^3$ V/cm, which are easily attainable. At temperatures $T\sim 10$ K, which is ordinarily the case in experiments of this kind (see, for example, Refs. 5 and 7), the thermal energy is approximately an order of magnitude smaller than the distance between the levels.

If the surface electron density $n_s\sim 10^{11}\,\mathrm{cm}^{-2}$, the Fermi level will lie above the ground state by an amount of the order of 10^{-3} eV, comparable to the thermal energy. Under these conditions most particles will be in the lower energy subband in one of the wells and will remain there until the ac field is switched on. The latter field can be produced using submillimeter-range lasers, which gives frequencies ω of the order of the transition frequency Δ.

In summary, estimates show that dynamical polarization effects in a double quantum well can be observed experimentally.

*)e-mail: burdov@phys.unn.rennet.ru

[1] F. Grossmann, T. Dittrich, P. Jung, and P. Hanggi, Phys. Rev. Lett. **67**, 516 (1991); F. Grossmann and P. Hanggi, Europhys. Lett. **18**, 571 (1992).
[2] R. Bavli and H. Metiu, Phys. Rev. Lett. **69**, 1986 (1992); Phys. Rev. A **47**, 3299 (1993).
[3] Y. Kayanuma, Phys. Rev. A **50**, 843 (1994).
[4] Y. Dakhnovskii and R. Bavli, Phys. Rev. B **48**, 11010 (1993); Y. Dakhnovskii, R. Bavli, and H. Metiu, Phys. Rev. B **53**, 4657 (1996).
[5] I. Brener, P. C. M. Planken, M. C. Nuss *et al.*, Appl. Phys. Lett. **63**, 2213 (1993).
[6] Y. Dakhnovskii and H. Metiu, Phys. Rev. B **51**, 4193 (1995).
[7] R. Aguado and G. Platero, Phys. Rev. B **55**, 12860 (1997).
[8] Ya. B. Zel'dovich, Zh. Éksp. Teor. Fiz. **51**, 1492 (1966) [Sov. Phys. JETP **24**, 1006 (1967)]; Usp. Fiz. Nauk **110**, 139 (1973) [Sov. Phys. Usp. **16**, 427 (1973)].
[9] V. A. Burdov, Zh. Éksp. Teor. Fiz. **112**, 1209 (1997) [JETP **85**, 657 (1997)].

Translated by M. E. Alferieff

Single-particle excitations and the order parameter for a trapped superfluid Fermi gas

M. A. Baranov
Kurchatov Institute Russian Research Center, 123182 Moscow, Russia

(Submitted 24 August 1999)
Pis'ma Zh. Éksp. Teor. Fiz. **70**, No. 6, 392–397 (25 September 1999)

It is found that the character of single-particle excitations of a trapped neutral-atom Fermi gas is strongly influenced by a superfluid phase transition. Below the transition temperature the presence of a spatially inhomogeneous order parameter (gap) shifts the excitation eigenenergies upward and leads to the appearance of in-gap excitations localized in the outer part of the gas sample. The eigenenergies become sensitive to the gas temperature and are no longer multiples of the trap frequencies. These features should manifest themselves in a strong change of the density oscillations induced by modulations of the trap frequencies and can be used for identifying the superfluid phase transition. [S0021-3640(99)00618-0]

PACS numbers: 05.30.Fk, 64.70.−p, 67.20.+k

The physics of ultracold trapped atomic gases has attracted a lot of attention after the discovery of Bose–Einstein condensation.[1–3] Trapped neutral-atom Fermi gases, when cooled to a sufficiently low temperature, should also exhibit prominent macroscopic quantum phenomena which are mostly related to a superfluid pairing phase transition. Possible versions of this phase transition in atomic samples have recently been discussed in Refs. 4–7. However, as only a small fraction of the particles is influenced by the pairing, it is not entirely clear how the transition will manifest itself in the dynamic and kinetic properties of the gas.

In this letter we indicate a clear way of identifying the pairing transition in a trapped Fermi gas. We study single-particle excitations and show that they are strongly influenced by the pairing. Above the transition temperature T_c the excitation eigenfrequencies are multiples of the trap frequencies. It turns out that below T_c the presence of the order parameter shifts the eigenenergies upward and creates conditions for the existence of in-gap excitations localized in the outer part of the gas sample in the well formed by the gap and the trapping potential. The eigenenergies become sensitive to the gas temperature and are no longer multiples of the trap frequencies. This should strongly change the response of the gas to modulations of the trap frequencies (see below).

The influence of pairing on single-particle excitations is essentially the same for all types of pairing discussed in Refs. 4–7, and for simplicity we confine ourselves to the case of the *s*-wave pairing. We consider a two-component neutral gas of fermionic atoms trapped in a spherically symmetrical harmonic potential. The two (hyperfine) components

labeled as α and β are assumed to have equal concentrations. The Hamiltonian of the system has the form ($\hbar=1$)

$$H=\sum_{i=\alpha,\beta}\int d\mathbf{r}\psi_i^+ H_0\psi_i+V\int d\mathbf{r}\psi_\alpha^+\psi_\alpha\psi_\beta^+\psi_\beta, \tag{1}$$

where $\psi_i(\mathbf{r})$ with $i=\alpha,\beta$ are the field operators of the α and β atoms, $H_0=-\nabla^2/2m+m\Omega^2r^2/2-\mu$, Ω is the trap frequency, and μ is the chemical potential which greatly exceeds Ω in the Thomas–Fermi limit (see e.g., Ref. 8) discussed below. The second term in Eq. (1) assumes an attractive elastic interaction between atoms in the states α and β (s-wave scattering length $a<0$); here $V=4\pi a/m$ is the coupling constant and m is the mass of an atom.

The presence of a negative s-wave scattering length for the intercomponent interaction leads to a superfluid phase transition via Cooper pairing in the s-wave channel,[6] with the critical temperature $T_c\ll\mu$. Being interested in the effect of this transition, we consider temperatures $T\ll\mu$, where the chemical potential coincides with the Fermi energy at the center of the trap: $\mu\approx\varepsilon_F=p_F^2/2m$, and the Thomas–Fermi radius of the gas sample $R_{TF}=v_F/\Omega$ serves as a unit of length ($v_F=p_F/m$). In this temperature range a small parameter of the theory is $\lambda=2|a|p_F/\pi\ll1$. The density profile of the gas is $n(R)=n_0(1-R^2)^{3/2}$, where $n_0=p_F^3/3\pi^2$ is the maximum gas density, and R the distance from the origin in units of R_{TF}. This density profile corresponds to the local Fermi momentum $p_F(R)=p_F(1-R^2)^{1/2}$, and the density of states on the local Fermi surface $N(R)=mp_F(R)/(2\pi^2)$. To be precise, the above formulas should be modified in the presence of the interaction. The leading mean-field corrections are smooth and small ($\propto\lambda$). They also result in a uniform shift of the particle eigenenergies in the vicinity of the chemical potential level. This shift can be absorbed by redefining μ.

We assume that the critical temperature T_c of the pairing transition is much larger than Ω and, hence, T_c is very close[7] to the critical temperature $T_c^{(0)}=0.28\varepsilon_F\times\exp(-1/\lambda)$ in a spatially homogeneous gas with density n_0 (Ref. 9). Below T_c the gas is characterized by the presence of the order parameter $\Delta(\mathbf{R})=|V|\langle\psi_\alpha(\mathbf{R})\psi_\beta(\mathbf{R})\rangle$. Following a standard mean-field procedure (see, e.g., Ref. 10), we can write the term describing the interparticle interaction in Eq. (1) in the form $\Delta(\mathbf{R})\psi_\alpha(\mathbf{R})\psi_\beta(\mathbf{R})+\Delta^*(\mathbf{R})\psi_\beta^\dagger(\mathbf{R})\psi_\alpha^\dagger(\mathbf{R})$. Then the Hamiltonian (1) becomes bilinear and can be reduced to a diagonal form by using the Bogolyubov transformation generalized for the spatially inhomogeneous case (Ref. 10):

$$\begin{pmatrix}\psi_\alpha(\mathbf{R})\\ \psi_\beta(\mathbf{R})\end{pmatrix}=\sum_\nu\left[U_\nu(\mathbf{R})\begin{pmatrix}\alpha_\nu\\ \beta_\nu\end{pmatrix}+V_\nu^*(\mathbf{R})\begin{pmatrix}\beta_\nu^\dagger\\ -\alpha_\nu^\dagger\end{pmatrix}\right],$$

where α_ν and β_ν are the operators of single-particle excitations. Their wave functions $U_\nu(\mathbf{R})$, $V_\nu(\mathbf{R})$ satisfy the Bogolyubov–de Gennes equations

$$H_0\begin{pmatrix}U_\nu\\ V_\nu\end{pmatrix}+\begin{pmatrix}\Delta(\mathbf{R})V_\nu\\ -\Delta^*(\mathbf{R})U_\nu\end{pmatrix}=\varepsilon_\nu\begin{pmatrix}U_\nu\\ -V_\nu\end{pmatrix}, \tag{2}$$

where $\varepsilon_\nu\geqslant0$ are the excitation energies.

In the vicinity of T_c the order parameter can be found from the Ginzburg–Landau equation:[7]

$$\Delta(R)=5.15\cdot T_c\sqrt{(T_c-T)/T_c}\,\exp(-R^2/2l_\Delta^2), \tag{3}$$

where $l_\Delta^2=\kappa\sqrt{2\lambda/(1+2\lambda)}\ll 1$, and $\kappa=0.13(\Omega/T_c)$. At lower temperatures, where the Ginzburg–Landau approach is not valid, $\Delta(R)$ can be obtained from the Eilenberger equations,[11] which in the presence of a harmonic trapping potential read

$$\begin{aligned} &ig'_\omega+(\Delta\cdot f_\omega-\Delta^*\cdot\tilde{f}_\omega)/\Omega=0,\\ &if'_\omega-(2i\omega f_\omega+2\Delta^*\cdot g_\omega)/\Omega=0,\\ &\tilde{i}f'_\omega+(2i\omega\tilde{f}_\omega+2\Delta\cdot g_\omega)/\Omega=0, \end{aligned} \tag{4}$$

where the prime symbol stands for the operator $(p_F(R)/p_F)(\mathbf{n}\cdot\nabla_{\mathbf{R}})$. Equations (4) follow from the well-known Gor'kov equations[12] under the assumption $\varepsilon_F(R)\gg T$. The functions f_ω, $\tilde{f}_\omega$, and g_ω depend on the position $\mathbf{R}$ and the unit vector $\mathbf{n}$, $f_\omega=f_\omega(\mathbf{R},\mathbf{n})$, etc., and obey the constraint $f_\omega(\mathbf{R},\mathbf{n})\tilde{f}_\omega(\mathbf{R},\mathbf{n})-g_\omega^2(\mathbf{R},\mathbf{n})=1/4$ (see Ref. 11 for more details).

Equations (4) must be completed by the self-consistency condition

$$\Delta(R)=|V|\cdot 2\pi N(R)T\sum_\omega\int\frac{d\mathbf{n}}{4\pi}f_\omega(\mathbf{R},\mathbf{n}), \tag{5}$$

where the summation is performed over the Matsubara frequencies $\omega=\pi T(2n+1)$.

For real Δ the function $\tilde{f}_\omega(\mathbf{R},\mathbf{n})=f_\omega(\mathbf{R},-\mathbf{n})$, and the solution of Eqs. (4) for f_ω, if the terms of order $(\Omega/\sqrt{T^2+\Delta^2})^3$ are omitted, can be written as

$$f_\omega=\frac{\Delta}{2\sqrt{\omega^2+\Delta^2}}+\frac{\omega}{4}\frac{\Omega\Delta'}{(\omega^2+\Delta^2)^{3/2}}+\Omega^2\left[\frac{\omega^2}{16}\frac{2(\omega^2+\Delta^2)\Delta''-5\Delta(\Delta')^2}{(\omega^2+\Delta^2)^{7/2}}\right], \tag{6}$$

where the prime has the same meaning as before. Equations (6) and (5) provide us with an equation for the order parameter $\Delta(R)$. Actually, the first term of Eq. (6) gives a formally divergent quantity $\Sigma_\omega\pi T/\sqrt{\omega^2+\Delta^2}$. To eliminate this divergency we renormalize the coupling constant V in the same way as has been done in the Bogolyubov method (see, e.g., Ref. 13). Then we obtain

$$\frac{\Delta}{\lambda N(R)}=\Delta\cdot\tilde{S}_{1/2}+S_{5/2}\frac{1-R^2}{12}\left[\frac{d^2\Delta}{dR^2}+\frac{1}{R}\frac{d\Delta}{dR}\frac{2-3R^2}{1-R^2}\right]-S_{7/2}\frac{5(1-R^2)}{24\Omega^2}\left(\frac{d\Delta}{dR}\right)^2\Delta, \tag{7}$$

where $S_\alpha\equiv\pi T\Sigma_\omega\omega^2/(\omega^2+\Delta^2)^\alpha$ for $\alpha=5/2,\ 7/2$, and

$$\tilde{S}_{1/2}=\frac{1}{\lambda}-\gamma-\ln\frac{\Delta}{\pi T_c^{(0)}(1-R^2)}-\int_0^\infty\frac{2dx}{\exp\left(\dfrac{\Delta}{T}\cosh(x)\right)+1},$$

with $\gamma=0.577$ being the Euler constant.

At T close to T_c equation (7) reduces to the Ginzburg–Landau equation from Ref. 7. For lower temperatures we solved Eq. (7) numerically, with the boundary conditions $\Delta'(0)=0$ and $\Delta(1)=0$. In Fig. 1 we present $\Delta(R)$ at various temperatures for $\lambda=0.3$ and $T_c^{(0)}=5\Omega$ ($T_c=0.86T_c^{(0)}$). A comparison with the results of the local-density approximation shows that the latter is adequate only at very low temperatures: with decreasing T,

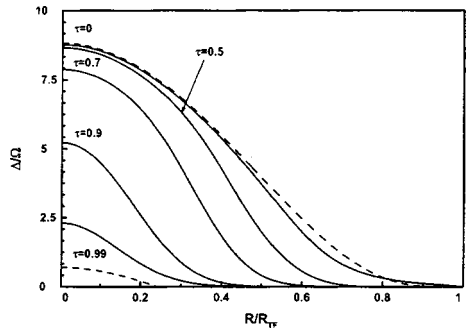

FIG. 1. Order parameter $\Delta(R)$ at various temperatures $\tau=T/T_c$ (solid lines). The dashed lines correspond to $\Delta(R)$ in the local density approximation at $\tau=0$ (upper curve) and $\tau=0.99$ (lower curve).

the spatial region in which Δ is substantially nonzero increases and, hence, the spatial derivatives of Δ, neglected in the local-density approximation, become less important.

In a spherically symmetrical trapping potential the elementary excitations are characterized by a radial quantum number n, orbital angular momentum l, and its projection m. The excitation wave functions can be written as $(U_\nu, V_\nu)=R^{-1}Y_{lm}(\hat{\mathbf{R}})\times[u_{nl}(R), v_{nl}(R)]$, where the functions (u,v) are normalized by the condition $\int_0^\infty (u_{nl}u^*_{n'l}+v_{nl}v^*_{n'l})dR=\delta_{nn'}$. At temperatures $T\ll\varepsilon_F\approx\mu$, elementary excitations formed by particles with energies in a narrow vicinity of the Fermi surface are most important. In the classically accessible region of space the excitation wave functions exhibit strong spatial oscillations, with a period of order $p_F^{-1}(R)\ll R_{TF}$ and a slowly varying amplitude $\tilde{u}_{nl}(R)$, $\tilde{v}_{nl}(R)$:

$$\begin{pmatrix} u_{nl} \\ v_{nl} \end{pmatrix} = \frac{\exp\left(i\tilde{\mu}\int_{R_1}^{R} p_{Fl}dR \right)}{\sqrt{p_{Fl}(R)}} \begin{pmatrix} \tilde{u}_{nl} \\ \tilde{v}_{nl} \end{pmatrix} + \text{h.c.}\ . \tag{8}$$

The partial Fermi momentum is defined as $p_{Fl}(R)=(1-R^2-(l+1/2)^2/\tilde{\mu}^2R^2)^{1/2}$, where $\tilde{\mu}=2\mu/\Omega\gg 1$, and the classically accessible region is specified by the condition $R_1<R<R_2$, with the turning points $R_{1,2}$ determined from the equation $p_{Fl}(R_{1,2})=0$. Omitting the terms of order $\tilde{\mu}^{-1}$ in Eq. (2), we obtain a pair of decoupled equations for the amplitudes $f_\pm=\tilde{u}\pm i\tilde{v}$ ($\hat{\varepsilon}_{nl}=\varepsilon_{nl}/\Omega\geqslant 0$, $\hat{\Delta}=\Delta/\Omega$):

$$\left[-\left(p_{Fl}\frac{d}{dR} \right)^2 + \hat{\Delta}^2 \pm p_{Fl}\frac{d\hat{\Delta}}{dR} - \hat{\varepsilon}_{nl}^2 \right] f_{nl\pm} = 0. \tag{9}$$

In the classically inaccessible regions $0<R<R_1$ (due to the centrifugal barrier) and $R>R_2$ (due to the trapping potential), Eqs. (9) must be modified by replacing $p_{Fl}(R)$ with $\mp i|p_{Fl}(R)|$, respectively, to obtain decaying solutions. Above T_c the order parameter is zero, and using a standard semiclassical procedure one can obtain the well-known result $E_{nl}^{(0)}=(2n+l+3/2)\Omega$ for the eigenenergies reckoned from the bottom of the potential well. In a spherical harmonic trap the chemical potential $\mu=(j+3/2)\Omega$, where j is

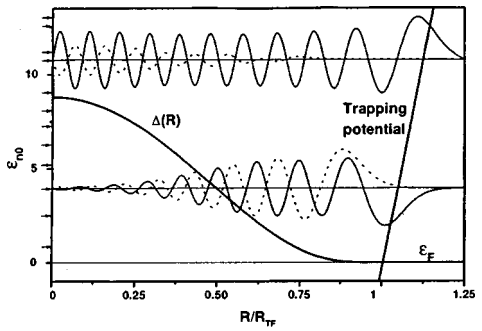

FIG. 2. Wave functions u_{n0} (solid lines) and v_{n0} (dashed lines) for above-gap and in-gap excitations, obtained by numerical solution of Eqs. (8) for $l=0$ at $T=0$. For illustrative purpose only (to reduce the number of rapid oscillations) we take $\tilde{\mu}=63$ instead of the actual value $\tilde{\mu}\approx 970$. The arrows indicate the eigenenergies of the excitations.

a positive integer. Accordingly, we obtain $\varepsilon_{nl}^{(0)}=|2n+l-j|\Omega$ for the eigenenergies of particlelike ($2n+l\geqslant j$, $\tilde{v}_{nl}=0$) and hole-like ($2n+l\leqslant j$, $\tilde{u}_{nl}=0$) single-particle excitations.

Below the transition point the appearance of the order parameter $\Delta(R)$ modifies the excitation spectrum. Just below T_c the order parameter is small and exists only in a small spatial region of radius $l_\Delta \ll 1$ [see Eq. (3)]. Therefore, the presence of $\Delta(R)$ only influences the excitations with small l and shifts their eigenenergies upward slightly: The shifts will be of order $\delta=\Delta(R_1)l_\Delta$, i.e., much smaller than the maximum value $\Delta(0)$ of the spatially inhomogeneous gap $\Delta(R)$. Hence, the lowest excitations, namely the ones with $\varepsilon_{nl}^{(0)}=0$ at $T>T_c$, become in-gap, i.e., have energies below the top of the gap: $\varepsilon_{nl}\sim\delta\ll\Delta(0)$. With decreasing temperature, $\Delta(R)$ grows rapidly, leading to an increase in the number of in-gap excited states.

At temperatures well below T_c the characteristic radius of $\Delta(R)$ becomes of the order the size of the gas sample R_{TF}, and all relevant excitations ($l\lesssim\tilde{\mu}/2$) are influenced by the presence of $\Delta(R)$. The wave functions of above-gap excitations [$\varepsilon_{nl}>\Delta(R_1)$] extend over the entire classically accessible region $R_1<R<R_2$. In contrast, the in-gap excitations with energies ε_{nl} well below $\Delta(R_1)$ are essentially ''expelled'' from the center of the trap: their wave functions are mostly localized in the well formed in the outer part of the sample by $\Delta(R)$ and the trapping potential (see Fig. 2).

For T well below T_c we have $\hat{\Delta}(0)\sim T_c/\Omega\gg 1$, and Eqs. (9) for the amplitudes $\tilde{u}_{nl}$, $\tilde{v}_{nl}$ can be solved in the semiclassical approach, omitting the terms with spatial derivatives of $\hat{\Delta}(R)$, as they are small compared to $\hat{\Delta}^2$. Then, in the spatial region where $\varepsilon>\Delta(R)$ we obtain

$$\begin{pmatrix}\tilde{u}_{nl}\\ \tilde{v}_{nl}\end{pmatrix}=\frac{\hat{\Delta}(R)}{\sqrt{\omega(R)}}\sum_{\pm}C_{\pm}\begin{pmatrix}\pm(\hat{\varepsilon}\mp\omega(R))^{-1/2}\\ \mp(\hat{\varepsilon}\pm\omega(R))^{-1/2}\end{pmatrix}\exp\left\{\pm i\int\frac{\omega(R)}{p_{Fl}(R)}dR\right\}. \tag{10}$$

Here $\omega(R)=\sqrt{\hat{\varepsilon}^2-\hat{\Delta}^2(R)}$, and $C_\pm$ are numerical coefficients. In the case of above-gap excitations [$\varepsilon_{nl}>\Delta(R_1)$] these coefficients can be found by making an analytical con-

tinuation of the solution (10) to the classically inaccessible regions $R<R_1$ and $R>R_2$. Since for $\varepsilon_{nl}>\Delta(R_1)$ there are only two (classical) turning points R_1 and R_2, the semiclassical quantization condition reads

$$\frac{2}{\pi}\int_{R_1}^{R_2}\frac{\sqrt{\varepsilon_{nl}^2-\Delta^2(R)}}{p_{Fl}(R)}dR=\varepsilon_{nl}^{(0)}. \tag{11}$$

This condition provides us with the energy spectrum of the above-gap excitations (see Fig. 2). The amplitudes $\tilde{u}_{nl}$, $\tilde{v}_{nl}$ of their wave functions oscillate in the entire region $R_1<R<R_2$ and decay in the classically inaccessible regions $R<R_1$ and $R>R_2$. Like the excitations above T_c, these excited states are twofold degenerate, but their energies are shifted upward by the presence of $\Delta(R)$.

For the in-gap excitations the situation is more subtle due to the appearance of a peculiar turning point R_c determined by the condition $\varepsilon_{nl}=\Delta(R_c)$. At this point a particle undergoes Andreev reflection[14] from the spatially inhomogeneous gap $\Delta(R)$ and transforms into a hole (and vice versa). As a result, these excitations acquire a superpositional particle–hole character and become nondegenerate, with a splitting that increases with $\Delta(0)$.

In the spatial region $R_c<R<R_2$ the amplitudes $\tilde{u}_{nl}$, $\tilde{v}_{nl}$ are determined by Eq. (10), with the coefficients $C_{\pm}$ following from an analytical continuation of Eq. (10) to the region $R_1<R<R_c$. In the latter region the amplitudes are given by the same Eq. (10) but in which $\omega(R)$ is replaced by $-i|\omega(R)|$ and the coefficients $C_{\pm}$ are obtained by making an analytical continuation to the classically inaccessible region $R<R_1$. As a result, the quantization condition for the in-gap excitations reads

$$(-1)^{j-l}\cos(2\phi)=2Z^2/(Z^4+1), \tag{12}$$

$$Z=\sqrt{2}\,\exp\left\{\int_{R_1}^{R_c}\sqrt{\Delta^2(R)-\varepsilon_{nl}^2}/p_{Fl}(R)dR\right\},\quad \phi=\int_{R_c}^{R_2}\sqrt{\varepsilon_{nl}^2-\Delta^2(R)}/p_{Fl}(R)dR.$$

The wave functions of these excitations are mainly localized in the region $R_c<R<R_2$, where the amplitudes $\tilde{u}_{nl}$ and $\tilde{v}_{nl}$ oscillate. For $R_1<R<R_c$ they decay exponentially. In fact, these amplitudes behave like wave functions of bound states in the potential well formed by the trapping potential on one side and by the order parameter $\Delta(R)$ on the other side (see Fig. 2). To a certain extent these excitations are analogous to localized states in the vortex core in ordinary superconductors.[15]

For the lowest in-gap excitations the semiclassical approach for finding the eigenenergies ε_{nl} and amplitudes $\tilde{u}_{nl}$, $\tilde{v}_{nl}$ is not adequate, and one has to solve Eq. (9) numerically. The energies of these excitations are very sensitive to $\Delta(R)$, and, hence, to the gas temperature. For $\Delta(R)$ in Fig. 1 at $T=0$ we find $\varepsilon_0=0.85\Omega$ for the lowest excitation with $l=0$ (Eq. (12) gives $\varepsilon_0=1.06\Omega$). With increasing T the value of ε_0 decreases ($\varepsilon_0=0.23\Omega$ for $T=0.99T_c$) and tends to zero for $T\to T_c$.

In conclusion, below the transition temperature, the excitation eigenfrequencies become temperature dependent and are no longer multiples of the trap frequencies. These features should lead to a strong change of the density oscillations induced by modulations of the trap frequency, which can be used for identifying the pairing transition. For example, spherically symmetrical modulations [$\delta\Omega\sim\cos(\nu t)$] cause single-particle transi-

tions between states with the same orbital angular momentum l, and above T_c the amplitude of the density oscillations will exhibit resonances at frequencies ν which are multiples of 2Ω. Below T_c the presence of $\Delta(R)$ changes the eigenfrequencies of some of the excitations, and those will not contribute to the density oscillations at the resonance frequencies. Hence, the resonance peaks broaden and become smaller. For $\Delta(R)$ in Fig. 1 the eigenfrequencies of all excitations with $l \lesssim \tilde{\mu}/2$ are altered by the pairing already at $T = 0.5T_c$. Thus the characteristic resonances present in the ν dependence of the density oscillations for the gas above T_c will now be smeared out. At low enough temperatures one should also expect the appearance of resonances related to collective modes of the order parameter. This issue will be addressed in a future publication.

I acknowledge fruitful discussions at the Quantum Collectief seminar in Amsterdam, and helpful conversations with G. V. Shlyapnikov, J. T. M. Walraven, and D. S. Petrov. This work was supported by the Stichting voor Fundamenteel Onderzoek der Materie (FOM), by INTAS, and by the Russian Fund for Fundamental Research (Grant 97-02-16532).

[1] M. H. Anderson, J. R. Ensher, M. R. Matthews *et al.*, Science **269**, 198 (1995).
[2] C. C. Bradley, C. A. Sackett, J. J. Tolett, and R. G. Hulet, Phys. Rev. Lett. **75**, 1687 (1995).
[3] K. B. Davis, M.-O. Mewes, M. R. Andrews *et al.*, Phys. Rev. Lett. **75**, 3969 (1995).
[4] H. T. C. Stoof, M. Houbiers, C. A. Sackett, and R. G. Hulet, Phys. Rev. Lett. **76**, 10 (1996).
[5] M. A. Baranov, Yu. Kagan, and M. Yu. Kagan, JETP Lett. **64**, 301 (1996).
[6] M. Houbiers, R. Ferwerda, H. T. C. Stoof *et al.*, Phys. Rev. A **56**, 4864 (1997).
[7] M. A. Baranov and D. S. Petrov, Phys. Rev. A **58**, R801 (1998).
[8] D. A. Butts and D. S. Rokhsar, Phys. Rev. A **55**, 4346 (1997).
[9] L. P. Gor'kov and T. K. Melik-Barkhudarov, Zh. Éksp. Teor. Fiz. **40**, 1452 (1961) [Sov. Phys. JETP **13**, 1018 (1961)].
[10] P. G. de Gennes, *Superconductivity of Metals and Alloys*, Addison-Wesley, Redwood City, Calif., 1989.
[11] G. Eilenberger, Zeitschr. für Phys. B **214**, 195 (1968).
[12] L. P. Gor'kov, Zh. Éksp. Teor. Fiz. **34**, 735 (1958) [Sov. Phys. JETP **7**, 505 (1958)].
[13] L. D. Landau and E. M. Lifshitz, *Statistical Physics*, Part 2, Pergamon Press, Oxford, 1980.
[14] A. F. Andreev, Zh. Éksp. Teor. Fiz. **46**, 1822 (1964) [Sov. Phys. JETP **19**, 1228 (1964)].
[15] C. Caroli, P. G. de Gennes, and J. Matricon, Phys. Lett. **9** , 307 (1964).

Published in English in the original Russian journal. Edited by Steve Torstveit.

Signatures of quantum chaos in the nodal points and streamlines in electron transport through billiards

K.-F. Berggren
Department of Physics and Measurement Technology, Linköping University, S-581 83 Linköping, Sweden

K. N. Pichugin
Kirensky Institute of Physics, 660036 Krasnoyarsk, Russia; Institute of Physics, Academy of Sciences, 16000 Prague, Czech Republic

A. F. Sadreev
Department of Physics and Measurement Technology, Linköping University, S-581 83 Linköping, Sweden; Kirensky Institute of Physics, 660036 Krasnoyarsk, Russia

A. Starikov
Kirensky Institute of Physics, 660036 Krasnoyarsk, Russia

(Submitted 30 August 1999)
Pis'ma Zh. Éksp. Teor. Fiz. **70**, No. 6, 398–404 (25 September 1999)

Streamlines and the distributions of nodal points are used as signatures of chaos in coherent electron transport through three types of billiards: Sinai, Bunimovich, and rectangular. Numerical averaged distribution functions of the nearest distances between nodal points are presented. We find the same form for the Sinai and Bunimovich billiards and suggest that there is a universal form that can be used as a signature of quantum chaos for electron transport in open billiards. The universal distribution function is found to be insensitive to the way the averaging is performed (over the positions of the leads, over an energy interval with a few conductance fluctuations, or both). The integrable rectangular billiard, on the other hand, displays a nonuniversal distribution with a central peak related to partial order of nodal points for the case of symmetric attachment of the leads. However, cases with asymmetric leads tend to the universal form. Also, it is shown how nodal points in the rectangular billiard can lead to ''channeling of quantum flows,'' while disorder in the nodal points in the Sinai billiard gives rise to unstable irregular behavior of the flow. © *1999 American Institute of Physics.* [S0021-3640(99)00718-5]

PACS numbers: 05.45.Mt, 72.10.−d

Billiards play a prominant role in the study of classical and quantum chaos.[1] Indeed, the nature of quantum chaos in a specific system is traditionally inferred from its its classical counterpart. Hence one may ask if quantum chaos is to be understood solely as a phenomenon that emerges in the classical limit, or are there some intrinsically quantal

phenomena that can contribute to irregular behavior in the quantum domain? This is a question we raise in connection with quantum transport through ideal regular and irregular electron billiards.

The seminal studies by McDonald and Kauffmann[2] of the morphology of eigenstates in a closed Bunimovich stadium have revealed characteristic patterns of disordered, nondirectional, and noncrossing nodal lines. Here we will first discuss what will happen to patterns like these when input and output leads are attached to a billiard, regular or irregular, and an electric current is induced through the the billiard by an applied voltage between the two leads. For such an open system the wave function ψ is now a scattering state with both real and imaginary parts, each of which gives rise to separate sets of nodal lines at which either $\mathrm{Re}[\psi]$ or $\mathrm{Im}[\psi]$ vanish. How will the patterns of nodal lines evolve as, e.g., the energy of injected electrons is increased, i.e., more scattering channels become open? Could they tell us something about how the perturbing leads reduce the symmetry and how an initially regular billiard may eventually turn into a chaotic one as the number of open modes increases? Below we will argue that nodal points, i.e., the points at which the two sets of nodal lines intersect because $\mathrm{Re}[\psi]=\mathrm{Im}[\psi]=0$, carry important information in this respect. Thus we will study their spatial distributions and try to characterize chaos in terms of such distributions. The question we wish to ask is simply if one can find a distinct difference between the distributions for nominally regular and irregular cavities.

In addition, what other signatures of quantum chaos may one find in the coherent transport in open billiards? The spatial distribution of nodal points plays a decisive role in how the flow pattern is shaped. Therefore we will also study the general behavior of streamlines derived from the probability current associated with a stationary scattering state

$$\psi=\sqrt{\rho}\,\exp(iS/\hbar).$$

The time-independent Schrödinger equation can be decomposed as[3,4]

$$E=\frac{1}{2}mv^2+V+V_{QM}, \quad \nabla\rho\mathbf{v}=0, \quad m\dot{\mathbf{X}}=\nabla S.$$

The separate quantum streamlines are sometimes referred to as Bohm trajectories.[4] In this alternative interpretation of quantum mechanics it is thought that an electron is a ''real'' particle that follows a continuous and causally defined trajectory (streamline) with a well-defined position $\mathbf{X}$, with the velocity of the particle given by the expressions above.

These equations imply that the electron moves under the influence of a force which is not obtained entirely from the classical potential V but also contains a ''quantum mechanical'' potential

$$V_{QM}=-\frac{\hbar^2}{2m}\frac{\nabla^2\rho}{\rho}.$$

This quantum potential is large and negative, where the wave function is small, and becomes infinite at the nodal points of the wave function where $\rho(x,y)=0$. Therefore, the close vicinity of a nodal point constitutes a forbidden area for quantum streamlines contributing to the net transport from source to drain. When ρ does not vanish, S is single-valued and continuous. However at the nodal point where $\psi=0$, neither S nor ∇S

is well defined. The behavior of S around these nodal points is discussed in Refs. 3, 5, and 6. For our study the main important property of the nodal points of ψ is that probability current flows described by ''open'' streamlines cannot encircle a nodal point. On the contrary, they are effectively repelled from the close vicinity of the nodal points, in a way as if these were impurities.

The scattering wave functions ψ are found by solving the Schrödinger equation in the tight-binding approximation with Neumann boundary conditions outside the billiards, at a distance over which the evanescent modes have effectively decayed to zero. The energy of the incident electron is $\epsilon=20$, where $\epsilon=2E_F d^2 m^*/\hbar$, with E_F the Fermi energy, d the width of the channel, and m^* the effective mass.

An inspection of the two sets of nodal lines associated with the real and imaginary parts of the scattering wave function reveals the typical pattern of nondirectional, self-avoiding nodal lines found previously by McDonald and Kaufman[2] for an isolated, irregular billiard. However, in our case of a complex scattering function the nodal lines are not uniquely defined, because multiplication of the wave function by an arbitrary constant phase factor $\exp(i\alpha)$ would yield a different pattern. The nodal points, on the other hand, appear to helpful in this respect. They represent a new aspect of the open system and will obviously remain fixed upon a change in the phase of the wave function. Here we conjecture that the nodal points may serve as unique markers which should prove useful for a quantitative characterization of scattering wave functions for open systems.

To be more specific, we have considered a large number of realizations (''samples'') of nodal points associated with different kinds of billiards and present averaged normalized distributions of nearest distances between the nodal points. Figure 1 shows the distributions for open Sinai (a), Bunimovich (b), and rectangular billiards (c, d). The distributions are obtained as an average over 101 different values of energy belonging to a specific energy window in which the conductance undergoes a few oscillations as shown by the insets in Fig. 1. Cases (a), (b), and (c) correspond to two-channel transmission through the billiards, while case (d) pertains to five-channel transmission. The rectangular billiard is nominally maximal in area with a numerical size 210×100 and with the width of the leads equal to 10.

It is noteworthy that the distribution of nearest neighbors is distinctly different from the corresponding distribution for random points in the two-dimensional plane,[7,8]

$$g(r)=2\pi\rho r\ \exp(-\pi\rho r^2), \tag{1}$$

where the density ρ of random points is related to the mean separation $\langle r\rangle$ as $\rho=1/4\langle r\rangle^2$. This distribution is shown in Fig. 1a by the thin line, indicating an underlying correlation between the nodal points of the transport wave function through the Sinai billiard. In this sense quantum chaos is not randomness.

With slight deviations the Bunimovich billiard gives rise to the same distributions as the Sinai, as shown by Fig. 1a and 1b. Analysis of the distributions for lower energies ($\epsilon\approx20$, one-channel transmission) gives quite similar universal forms, as shown in Fig. 1a and 1b, but with more pronounced fluctuations because the number of nodal points is smaller at lower energies. Moreover, averaging over wider energy domains with a finer

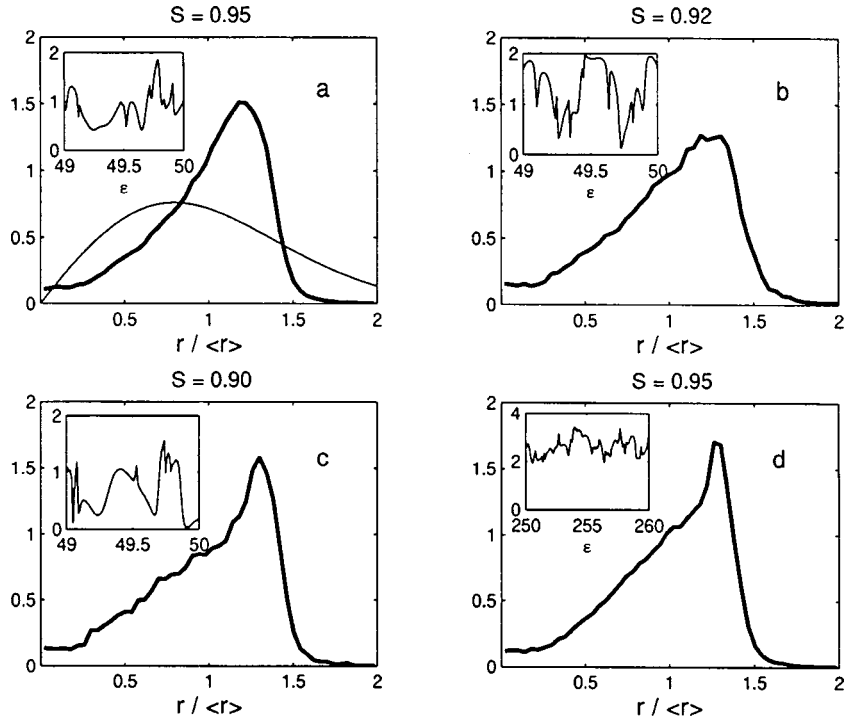

FIG. 1. Normalized distributions for nearest separations between nodal points (in units of the mean separation) averaged over an energy window for the chaotic Sinai (a) and Bunimovich billiards (b) and for two rectangular billiards (c, d). The Shannon entropy S is given for each separate case. Cases (a), (b), and (c) correspond to two-channel transmission and case (d) to five open channels. The corresponding conductance (in units of $2e^2/h$) versus energy is shown in the insets, which also define the energy window for each case. The distribution (1) for the nearest distances among completely random points is shown by thin line in (a).

grid or for higher energies gives no visible deviations from the distributions in Fig. 1a and 1b.

We considered also the Berry wave function of a chaotic billiard, which is accepted as a standard measure of quantum chaos:[9]

$$\psi(x,y)=\sum_j |a_j|\exp[ik(\cos\theta_j x+\sin\theta_j y)+\phi_j], \tag{2}$$

where $\theta_j, |a_j|$ and ϕ_j are independent random variables. We found that the distribution of nearest distances between the nodal points of (2) has completely the same form as for the Sinai billiard (Fig. 1a). On the other hand, an analysis of the nodal points of the wave function

$$\psi(x,y)=\sum_{k_x,k_y} \exp(ik_x x+k_y y) \tag{3}$$

with k_x, k_y distributed randomly leads to the distribution (1) of random points.

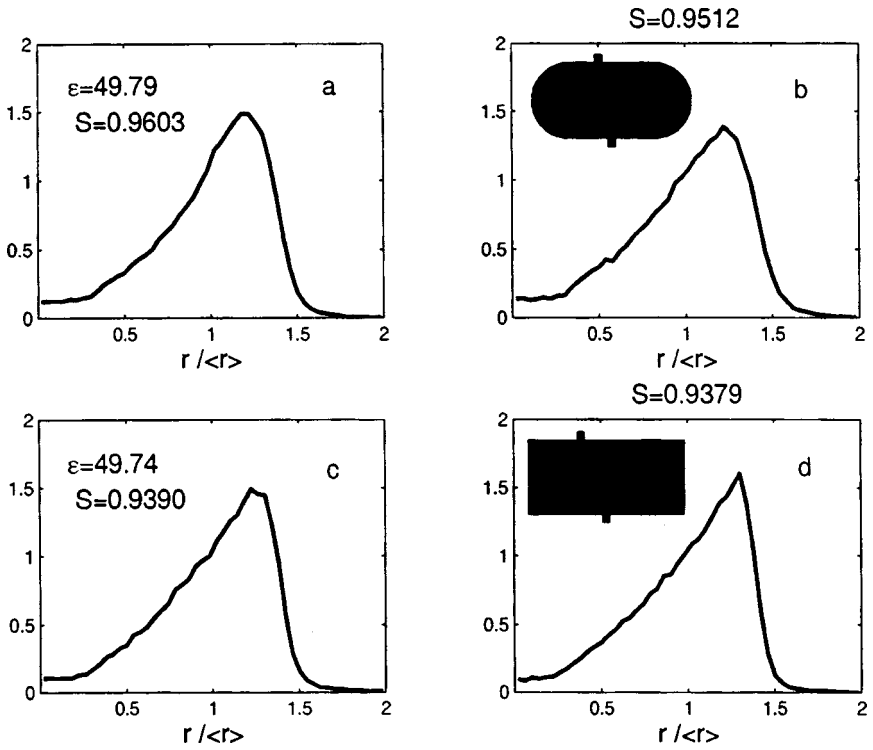

FIG. 2. Normalized distributions averaged over position of input lead for the Sinai billiard (a), over an energy window from ϵ=49 to 50 for the Bunimovich billiard with asymmetric input lead (b), over lead positions for the rectangular billiard (c), and over an energy window for the rectangular billiard with asymmetric input lead (d).

To supplement the averaging over energy we have also considered the positions of the leads. Figure 2a shows the normalized distribution of the nearest distances between nodal points for the Sinai billiard, obtained as an average over 101 positions of the input lead. It is seen that this distribution has the same form as the energy-averaged Sinai billiard in Fig. 1a. In the same way Fig. 2b shows the corresponding case of the Bunimovich billiard with an asymmetric input lead; this is to be compared with Fig. 1b. The asymmetric arrangement of leads allows a larger number of eigenstates of the Bunimovich billiard to participate in the electron transport because symmetry restrictions are relaxed.[10]

On the basis of Figs. 1 and 2 and comparison with the Berry wave function (2) we therefore argue that there is a universal distribution that characterizes open chaotic billiards. At this stage we conclude that the form of the distributions is insensitive to the averaging procedure, to the number of channels of electron transmission, and to the type of attachment of the leads. The mathematical form of the universal distribution constitutes an interesting problem that remains to be solved. So does a derivation of the random distribution associated with wave function in Eq. (3).

Let us now turn to the case of the nominally regular rectangular billiard. In Fig. 1c the distribution functions are given for the case of two-channel transmission with the

same energy-averaging procedure as for the chaotic billiards. The nearest-neighbor distribution clearly displays a peak corresponding to a regular set of nodal points, in contrast to the other billiards discussed above. This feature is found even for very high energies around 250 (five-channel transmission). Therefore the rectangular dot with the two symmetrically attached leads displays considerable stability with respect to regular nodal points, in contrast to the chaotic Sinai and Bunimovich billiards.

As indicated, symmetric leads impose restrictions on how states inside the billiard are selected and mixed on injection of a particle. In Fig. 2c the result of averaging over the positions of the input lead is therefore shown for the rectangular billiard at a fixed energy chosen from the energy domain in Fig. 1c. As one might expect, the pronounced peak in the distribution function of nearest nodal points has now disappeared. Moreover, the distribution is close to the case of the Bunimovich billiard in Figs. 1b and 2b. Evidently the asymmetrical positioning of the leads disturbs the nominally regular billiard in a much more profound way, effectively lending it chaotic characteristics. To reconfirm this conclusion we have also performed calculations of the distribution of nodal points within the same energy domain and with the same number of energy steps as in Fig. 1c but for non symmetrical positions of the input lead. In fact, the distribution function of nearest distances in Fig. 2d demonstrates a close similarity with the position average of the nodal points. Therefore the nonuniversal behavior of the distribution function of nodal points for the rectangular billiard shown in Fig. 1c and 1d is the result of the fact that only a few symmetrical eigenstates take part in the transmission because of symmetry restrictions.

In order to give a quantitative measure of the disorder of nodal point patterns we consider the Shannon entropy S (Ref. 11) normalized for each specific billiard by the entropy of completely random points. Numerical values for S are specified in Figs. 1 and 2. As one might expect, for the same energy window there is a clear tendency towards maximal entropy for chaotic billiards. A similar tendency is clearly seen for the position average (Fig. 2). The case of a rectangular billiard with entropy 0.95 (Fig. 1d) is beyond the scope of this rule, because for five-channel transmission the number of nodal points substantially exceeds that for the other cases considered, irrespective of the type of billiard. Thus the Shannon entropy of nodal points is an important additional quantitative measure of quantum chaos for quantum transport through billiards.

As we have said, the streamlines are strongly affected by the positions of the nodal points. Superficially they play the role of impurities. It is therefore of interest to determine whether the streamlines behave differently for regular and irregular situations, and for this reason we will consider a few typical examples, starting with two well-defined systems: the nominally regular rectangle and the irregular Sinai billiard. Figure 3a shows the flow lines in the case of the rectangular billiard. The features of the flow lines connecting the input and output leads are remarkable. It is clearly seen how the flow (trajectories) effectively ''channel'' through a ''nodal crystal,'' avoiding the individual nodal points. This picture is evidently very different from semi-classical physics and periodic orbit theory.[12] In Fig. 3 only contributions to the net current are displayed. In addition there are also vortical motions centered around each nodal point.

The other extreme, the completely chaotic Sinai billiard, is shown in Fig. 3b. Because the nodal distribution is now irregular also, the streamlines form an irregular pattern when finding their way through the rough potential landscape. Since a streamline

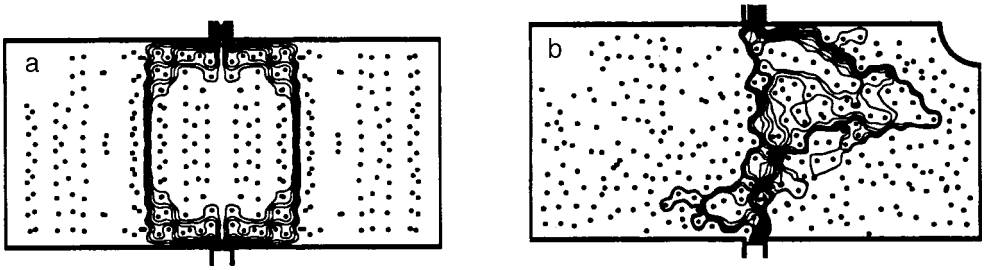

FIG. 3. Streamlines and positions of vortices (nodal points) at maximum conductance ($2e^2/h$) for (a) the rectangle with $\epsilon=20.44$ and (b) for the Sinai billiard with $\epsilon=20.79$.

cannot cross itself, Fig. 3 brings to mind the classical example of meandering rivers in a flat delta landscape. As is well known, slight changes in the topography, for example, by moving only a few obstacles to new positions, may induce completely new flow patterns in a sometimes dramatic ways. In the same way slight variations of the energy, for example, may affect the quantum streamlines in the Sinai billiard in an endless way, occasionally forming more collected bunches connecting the two leads in a more focused way than in Fig. 3b. The same type of behavior has also been obtained for a two-dimensional ring in which a tiny variation of the external magnetic flux induce drastic changes of the flow lines and, as a consequence, the Aharonov–Bohm oscillations become irregular.[13]

This work has been partially supported by the INTAS-RFBR Grant 95-IN-RU-657, RFFI Grant 97-02-16305, and the Swedish Natural Science Research Council. The computations were in part performed at the National Supercomputer Center at Linköping University.

[1] T. Guhr, A. Müller-Groeling, and H. A. Weidenmüller, Phys. Rep. **299**, 189 (1998).
[2] S. W. McDonald and A. N. Kaufman, Phys. Rev. Lett. **42**, 1189 (1979); Phys. Rev. A **37**, 3067 (1988).
[3] J. O. Hirschfelder, C. J. Goebel, and L. W. Bruch, J. Chem. Phys. **61**, 5456 (1974).
[4] P. R. Holland, *The Quantum Theory of Motion. An Account of the de Broglie-Bohm Causal Interpretation of Quantum Mechanics*, Cambridge University Press, Cambridge, 1993.
[5] H. Wu and D. W. L. Sprung, Phys. Lett. A **183**, 413 (1993).
[6] P. Exner, P. Šeba, A. F. Sadreev *et al.*, Phys. Rev. Lett. **80**, 1710 (1998).
[7] B. I. Shklovskii and A. L. Efros, *Elctronic Properties of Doped Semiconductors*, Chapter 3, Springer-Verlag, Berlin–New York, 1984.
[8] J. R. Eggert, Phys. Rev. B **29**, 6664 (1984).
[9] M. V. Berry, Philos. Trans. R. Soc. London, Ser. A **287**, 237 (1971).
[10] I. V. Zozoulenko and K.-F. Berggren, Phys. Rev. B **56**, 1 (1997).
[11] A. Garcimartin, A. Guarino, L. Bellon, and S. Giliberto, Phys. Rev. Lett. **79**, 3202 (1997).
[12] M. Brack and R. K. Bhaduri, *Semiclassical Physics*, Addison-Wesley, Reading, Mass., 1997.
[13] K. N. Pichugin and A. F. Sadreev, Phys. Rev. B **56**, 9662 (1997).

Published in English in the original Russian journal. Edited by Steve Torstveit.

Landau quantization and equatorial states on the surface of a nanosphere

D. N. Aristov
St. Petersburg Nuclear Physics Institute, 188350 Gatchina, Leningrad Region, Russia

(Submitted 31 August 1999)
Pis'ma Zh. Éksp. Teor. Fiz. **70**, No. 6, 405–409 (25 September 1999)

The Landau quantization for the electron gas on the surface of a sphere is considered. It is shown that in the regime of strong fields the lowest energy states are those with magnetic quantum numbers m of order of Φ/Φ_0, the number of magnetic flux quanta piercing the sphere. For an electron gas of low density (semiconducting situation) it leads to the formation of an electronic stripe on the equator of the sphere in high fields. © *1999 American Institute of Physics.*
[S0021-3640(99)00818-X]

PACS numbers: 73.20.Dx, 71.10.Ca

The electronic properties of cylindrical and spherical nanosize objects have attracted much theoretical interest in recent years. This interest is mostly related to the physics of carbon macromolecules and, in particular, to the transport properties of carbon nanotubes.[1] One encounters spherical nanosize objects in studies of the nonlinear optical response in composite materials,[2] of simple metal clusters,[3] and of photonic crystals based on synthetic opals.[4] In the most of these studies, the coating of the nanosphere is characterized by an effective dielectric function.[5] It has been noted, however,[6] that this approach must be revised if the coating of a sphere has a width of a few monolayers, a limit which is attainable by modern technologies.

In recent papers we have considered the electron gas on a sphere. We showed that various correlation functions in such a gas exhibit maxima when the electrons are at the antipodal points (north and south poles).[7] The exact solution was found for a problem in a uniform magnetic field, and the limits of weak and high fields were investigated.[8] In the high-field regime the formation of Landau levels was demonstrated. The complexity of the special functions describing the exact solution, however, complicates the analysis of the physical picture in the high-field regime. In this paper we explore qualitative arguments, supported by numerical calculations, to clarify the issue. We find that the minimum energy of the Hamiltonian is provided by the electronic states located near the equator of the sphere. For low densities of the gas one thus expects that a high field will push the electrons toward the equator and form an electronic ring there.

We consider the electron gas moving within a thin layer on the surface of a sphere of radius r_0. We assume a Hamiltonian of the form $\mathcal{H}=-\nabla^2/2m_e+U(r)$, where m_e is the electron mass. The chemical potential μ determines the total number of electrons N (with one projection of spin) and their areal density $\nu=N/4\pi r_0^2$. The confining quantum-

well potential $U(r)$ restricts the radial motion within a thin layer $\delta r \ll r_0$. We are interested in the case $\delta r < \nu^{-1/2}$, when the first excited state of the radial motion lies above the chemical potential. Then one can ignore the radial component of the wave function and put $r = r_0$ in the remaining angular part of the Hamiltonian. In the absence of magnetic field we have $\mathcal{H}_\Omega^{(0)} = -(2m_e r_0^2)^{-1}\Delta_\Omega$, with Δ_Ω being the angular part of the Laplacian. The solutions to this Hamiltonian are the spherical harmonics Y_{lm}, and the spectrum is that of a free rotator model :

$$\Psi^{(0)}(\theta,\phi) = r_0^{-1} Y_{lm}(\theta,\phi), \quad E_l^{(0)} = (2m_e r_0^2)^{-1} l(l+1).$$

In the presence of a uniform magnetic field **B** directed toward the north pole of the sphere ($\theta = 0$) we choose the gauge of the vector potential as $\mathbf{A} = \frac{1}{2}(\mathbf{B} \times \mathbf{r})$. Then the angular part $\mathcal{H}_\Omega$ of the Hamiltonian

$$\mathcal{H} = \frac{1}{2m_e}(-i\nabla + e\mathbf{A})^2 + U(r)$$

acquires the form

$$\mathcal{H}_\Omega = (2m_e r_0^2)^{-1}\left[-\Delta_\Omega + 2ip\frac{\partial}{\partial\phi} + p^2\sin^2\theta\right]. \tag{1}$$

The governing parameter here is $p = \pi B r_0^2/\Phi_0$, with the magnetic flux quantum $\Phi_0 = 2 \times 10^{-15}\ \mathrm{T\cdot m^2}$. For a sphere of radius $r_0 = 100$ nm one has $p = 1$ at a field $B \simeq 600$ Oe. The solutions of (1) are given by the oblate (angular) spheroidal functions and were analyzed in Ref. 8 to some detail.

In the weak-field regime, $p \sim 1$, jumps in the static magnetic susceptibility χ at half-integer p were demonstrated. The amplitude of these jumps is parametrically larger than the Pauli spin contribution and decreases with the increase of p. It was shown that the weak-field regime ends at $p^2 \sim p_c^2 = 2\sqrt{N}$. For $r_0 \sim 100$ nm (the case of opals) and in the metallic situation, e.g., at the densities $\nu \sim 10^{14}\,\mathrm{cm}^{-2}$, we have $N \sim 10^5$ and $p_c \simeq 30$.

On the other hand, at the lower (semiconducting) densities, $\nu \sim 10^{10}\,\mathrm{cm}^{-2}$, we have $N \sim 10$. Formally in this case $p_c \simeq 3$, i.e., the field is no longer small at p of the order of unity. The jumps in the susceptibility were predicted in Ref. 8 on the assumption that $\sqrt{N} \gg 1$, which is violated in the latter case of lower ν. At the same time, the experimentally accessible fields of the order of 6 T result in $p \sim 100$ for spheres with $r_0 \sim 100$ nm, i.e., we come into the strong field regime.

For strong fields, $p \to \infty$, one observes the eventual formation of Landau levels (LL). The spherical geometry brings into the problem some peculiarities which were partly discussed in Ref. 8. First is the incomplete restructuring of the spectrum into the LL scheme. This restructuring takes place only for levels with initial momentum l lower than p, and the field remains weak for the levels with $l > p^2$. Secondly, the field-induced double-well potential $p^2\sin^2\theta$ in (1) localizes the electron states with moderate magnetic quantum numbers m ($|m| \ll p$) near the poles $\theta = 0$ and $\theta = \pi$. As a result, only correlations within one hemisphere survive. Specifically, if an electron was initially in the northern hemisphere, then the probability of finding it in the southern hemisphere is exponentially small.

At the same time, the spherical geometry produces yet another effect which we shall now discuss. The effective potential in the strong-field regime can be written as

$$U_{\rm eff}(\theta)=\frac{p\omega_c}{4}\left(\frac{m/p}{\sin\theta}+\sin\theta\right)^2, \tag{2}$$

with the cyclotron frequency $\omega_c=eB/m_e$. At small negative m we have two minima of $U_{\rm eff}(\theta)$ near $\theta_0=\arcsin(\sqrt{|m|/p})$ and $\theta_0=\pi-\arcsin(\sqrt{|m|/p})$, where we expand

$$U_{\rm eff}(\theta_0+\theta)\simeq(\omega_c p\,\cos^2\theta_0)\,\theta^2. \tag{3}$$

Performing the rescaling $\theta\to x/\sqrt{2p|\cos\theta_0|}$ here, we arrive at a quantum oscillator problem of the form

$$\mathcal{H}\simeq\frac{\omega_c|\cos\theta_0|}{2}(-d^2/dx^2+x^2),$$

i.e., the well-known Landau quantization. As long as $|\cos\theta_0|\sim 1$, the wave-functions are extended at the scale $|\theta-\theta_0|\sim p^{-1/2}$. The possibility of quantum tunneling between θ_0 and $\pi-\theta_0$ produces the exponentially small splitting between the states centered at these points.[8]

Thus we see that the energy levels are labeled by two quantum numbers, a magnetic number m and LL number n, with approximate twofold degeneracy for given m,n.

This simple picture becomes inadequate when $|m|\simeq p$ and $\theta_0\simeq\pi/2$. In this case the harmonic potential in (3) weakens, which makes necessary the consideration of the fourth-order terms in the expansion. We have in this case

$$U_{\rm eff}\left(\theta+\frac{\pi}{2}\right)\simeq\frac{\omega_c p}{4}\theta^4,\quad |m|=p. \tag{4}$$

Now rescaling $\theta\to xp^{-1/3}$, we arrive at the following Schrödinger equation:

$$\frac{\omega_c}{4p^{1/3}}(-d^2/dx^2+x^4)\psi=E\psi.$$

The solution of the last equation apparently is not known.[9] For our purposes it suffices to note that the energy scales as $\omega_c/p^{1/3}\ll\omega_c$, and the wave functions on the equator extend over a scale of $|\theta-\pi/2|\sim p^{-1/3}$. In addition, we no longer have a double-well potential, and the energy levels are separated by the same scale $\omega_c/p^{1/3}$. The cross-over between Eqs. (3) and (4) takes place at $1-|m|/p\sim p^{-2/3}$.

With further increase of $|m|$, at $|m|>p$, the minimum value of $U_{\rm eff}$ is found at $\theta=\pi/2$ and increases rapidly with $|m|$. In this case the energy levels are $E_{lm}\sim\omega_c(m+p)^2/p$ and thus lie well above those with $|m|<p$.

Let us illustrate these qualitative results using the results of numerical calculations. We found the spectrum of Eq. (1) by diagonalizing $\mathcal{H}_\Omega$ in the basis of Legendre polynomials $P^m_{m+n}(\cos\theta)$ with $0\leqslant n\leqslant 200$ (Ref. 10). The results are shown in Fig. 1. One verifies that the ''equatorial'' states with $|m|\simeq p\gg 1$ provide the minimum eigenvalues of the Hamiltonian. This dependence of the energy level scheme on m is probably of minor importance if we consider the situation of a metal,[8] where the chemical potential lies well above the bottom of the conduction band ($\mu\gg\omega_c$). In this case the number of electrons

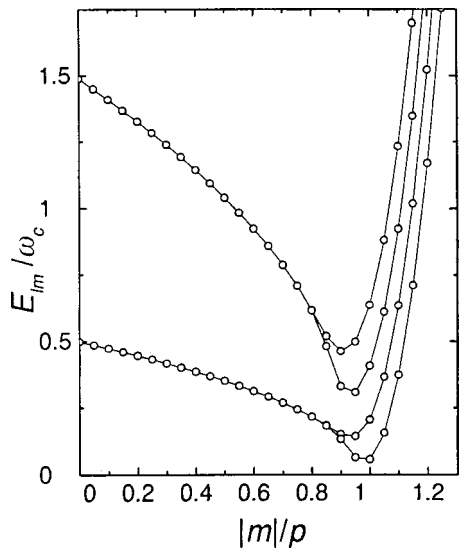

FIG. 1. The dependence of the four lowest energy levels E_{lm} on the magnetic number $m<0$ in the high-field regime, $p=\Phi/\Phi_0=100$. The calculated points are shown by circles; the lines are a guide to the eye.

N on the sphere is expected to exceed the number of flux quanta p. Then several Landau levels are occupied (several lines in Fig. 1) and the electrons are distributed over the whole sphere.

At the same time, the semiconducting coating of the sphere can lead to a different result. Indeed, if the cyclotron frequency ω_c is high enough, then the ''polar'' states with small negative m are poorly occupied. Meanwhile, the ''equatorial'' states with energies $\sim\omega_c p^{-1/3}$ are occupied to a larger extent. This produces an effective ring on the equator of the sphere. The criterion for this phenomenon is $N\lesssim p$ or, equivalently, $B\gtrsim\Phi_0\nu$. Note that the latter inequalities correspond to the partially filled lowest Landau level in the usual planar geometry.

We see that in the spherical geometry of the electron gas the states with higher $|m|$ possess the lower energy. Our situation is thus opposite to the one discussed for the quantum Hall edge states.[11] Nevertheless both problems have a common ingredient, the linear-in-m spectrum for a given n (in our case in two domains, $|m|\lesssim p$ and $|m|\gtrsim p$). Having effectively a case of one spatial dimension, we can consider the interaction effects as well. The problem has a certain subtlety, however, which is described below.

In certain cases one may hope to ignore the interaction between states belonging to different ''Landau levels'' (different curves in Fig. 1). Considering now the lowest LL, one observes familiar branches of right- and left-going fermions, $|m|\lesssim p$ and $|m|\gtrsim p$, with the negative and positive ''Fermi velocities'' $v_F=dE_{lm}/dm$, respectively. The absolute values of v_F for left and right movers are different. This point alone makes it difficult to pass to a bosonization description with one scalar field for both movers, and the notion of the chiral Luttinger liquid arises. A thorough consideration of the latter problem is beyond the scope of this study.

In conclusion, we have considered the Landau quantization for the electron gas on

the surface of a sphere. The exact solution of this problem involves complicated functions, which are not very instructive for the analysis of states with large magnetic numbers m for the electron motion. We have elucidated the role of the ''equatorial'' states with large m both analytically and numerically. Since these states are lower in energy, the electronic stripe on the equator can be realized for the semiconducting coating of the sphere in high magnetic fields.

I thank S. G. Romanov, A. G. Yashenkin, K. Hansen, V. A. Kulbachinskii for helpful discussions and communications. The financial support from the Russian State Program for Statistical Physics (Grant VIII-2), Grant FTNS 99-1134, and Grant INTAS 97-1342 is gratefully acknowledged.

[1] Y. Miyamoto, S. G. Louie, and M. L. Cohen, Phys. Rev. Lett. **78**, 2811 (1997); H. Yoshioka and A. A. Odintsov, Phys. Rev. Lett. **82**, 374 (1999).
[2] N. A. Nicorovici, R. C. McPhedran, and G. W. Milton, Phys. Rev. B **49**, 8479 (1994); K. W. Yu, P. M. Hui, and D. Stroud, Phys. Rev. B **47**, 14150 (1993).
[3] For a review, see W. A. de Heer, Rev. Mod. Phys. **65**, 611 (1993).
[4] S. G. Romanov, N. P. Johnson, A. V. Fokin *et al.*, Appl. Phys. Lett. **70**, 2091 (1997); Yu. A. Vlasov, V. N. Astratov, and O. Z. Karimov *et al.*, Phys. Rev. B **55**, R13357 (1997); H. Miguez, A. Blanco, F. Meseguer *et al.*, Phys. Rev. B **59**, 1563 (1999).
[5] D. J. Bergman, O. Levy, and D. Stroud, Phys. Rev. B **49**, 129 (1994).
[6] W. Ekardt, Phys. Rev. B **34**, 526 (1986).
[7] D. N. Aristov, Phys. Rev. B **60**, 2851 (1999).
[8] D. N. Aristov, Phys. Rev. B **59**, 6368 (1999).
[9] E. Kamke, *Gewöhnliche Differentialgleichungen*, Akad. Verlag, Leipzig, 1959.
[10] C. Flammer, *Spheroidal Wave Functions*, Stanford University Press, Stanford, 1957.
[11] X. G. Wen, Phys. Rev. B **41**, 12838 (1990); **43**, 11025 (1991).

Published in English in the original Russian journal. Edited by Steve Torstveit.